arXiv:1412.6672v2 [cond-mat.quant-gas] 23 Jun 2016

Competing Orders in a Dipolar Bose-Fermi Mixture on a Square Optical Lattice: Mean-Field Perspective

Jasen A. Scaramazza,[1,2] Ben Kain,[3] and Hong Y. Ling[1,4,5]

[1] *Department of Physics and Astronomy, Rowan University, Glassboro, New Jersey 08028, USA*
[2] *Department of Physics and Astronomy, Rutgers University, Piscataway, New Jersey 08854, USA*
[3] *Department of Physics, College of the Holy Cross, Worcester, Massachusetts 01610, USA*
[4] *Kavli Institute for Theoretical Physics, University of California, Santa Barbara, California 93106, USA*
[5] *ITAMP, Harvard-Smithsonian Center for Astrophysics, Cambridge, Massachusetts 02138, USA*

We consider a mixture of a two-component Fermi gas and a single-component dipolar Bose gas in a square optical lattice and reduce it into an effective Fermi system where the Fermi-Fermi interaction includes the attractive interaction induced by the phonons of a uniform dipolar Bose-Einstein condensate. Focusing on this effective Fermi system in the parameter regime that preserves the symmetry of D_4, the point group of a square, we explore, within the Hartree-Fock-Bogoliubov mean-field theory, the phase competition among density wave orderings and superfluid pairings. We construct the matrix representation of the linearized gap equation in the irreducible representations of D_4. We show that in the weak coupling regime, each matrix element, which is a four-dimensional (4D) integral in momentum space, can be put in a separable form involving a 1D integral, which is only a function of temperature and the chemical potential, and a pairing-specific "effective" interaction, which is an analytical function of the parameters that characterize the Fermi-Fermi interactions in our system. We analyze the critical temperatures of various competing orders as functions of different system parameters in both the absence and presence of the dipolar interaction. We find that close to half filling, the $d_{x^2-y^2}$-wave pairing with a critical temperature in the order of a fraction of Fermi energy (at half filling) may dominate all other phases, and at a higher filling factor, the p-wave pairing with a critical temperature in the order of a hundredth of Fermi energy may emerge as a winner. We find that tuning a dipolar interaction can dramatically enhance the pairings with d_{xy}- and g-wave symmetries but not enough for them to dominate other competing phases.

1. Introduction

Low-temperature crystal solids are full of wonderful and surprising phenomena, that are of both fundamental and practical importance but often difficult to observe owing to the imperfect nature and inflexibility of solid state systems. Free of these shortcomings, cold atoms, offer a pristine and highly controllable environment for creating novel quantum matter. Experimental realization of the superfluid–Mott insulator transition, a quintessential condensed matter phenomenon, in cold atom lattices [1] as exactly predicted by theory [2, 3] serves as one of many remarkable examples. It is experimental developments like this, along with the ability to create cold atom lattices that meet virtually any need, that has motivated tremendous activity in the past decade in using cold atom lattice models as an excellent platform for exploring and mimicking complicated condensed matter phenomena [4].

A subject of profound importance in condensed matter physics is superconductivity, a coherent phenomenon arising from condensation of correlated electron pairs, also known as Bardeen-Cooper-Schriffer (BCS) pairs, on a macroscopic scale. A BCS pair, however, is not energetically favored unless there exists an attraction between its constituents, which appears impossible in an electron system where Coulomb repulsion dominates. The effort to solve this mystery led, through the insights of Flölich, to the phonons of ionic crystal lattice oscillations and the eventual understanding that the interaction they induce between electrons is the source of the attraction responsible for superconductivity in most materials [5].

In cold atom physics, an analogous situation can arise from a Bose-Fermi mixture, where phonons can exist as low energy excitations of a Bose-Einstein condensate (BEC), describing the density fluctuation of the BEC [6]. The same phonons in the Bose gas can then induce an attractive interaction between fermions in the Fermi gas [6]. This, along with the unprecedented ability to tune parameters in such systems, e.g., two-body interaction and dimensionality, allows for the possibility of clean and controllable realization (or quantum simulation) of superfluid pairings in cold atom Bose-Fermi mixtures [7, 8].

Remarkable experimental progress has been made in creating quantum-degenerate Bose-Fermi mixtures, e.g., ^{7}Li-^{6}Li [9, 10], ^{23}Na-^{6}Li [11], ^{87}Rb-^{40}K [12–15], ^{6}Li-^{87}Rb [16], and ^{23}Na-^{40}K [17]. Most recently, a mixture where both bosons and fermions are in the superfluid state has been realized [18]. These developments together with the recent upsurge of experimental efforts in achieving dipolar quantum gases, in systems with ^{40}K^{87}Rb [19–21], ^{6}Li^{40}K [22–24], and ^{23}Na^{40}K [25] heteronuclear molecules, ^{87}Rb spinor condensates [26], and ^{32}Cr [27], ^{164}Dy [28] and ^{168}Er [29] atoms, has opened up the exciting possibility of creating dipolar Bose-Fermi mixtures with intriguing and unique properties. Of particular relevance to the present work is a Bose-Fermi mixture involving a two-component Fermi gas, examples

of which include the mixture of bosonic ^{41}K with two fermionic species ^{40}K and ^{6}Li [30], Feshbach molecules with two lowest hyperfine states of the same fermionic species ^{6}Li [31], and ground state ^{6}Li^{40}K molecules with two fermionic species ^{6}Li and ^{40}K [22–24]. The last one is particularly motivating since the ground ^{6}Li^{40}K molecules are bosons with a large dipole moment of 3.6 Debye. In a dipolar BEC [32, 33], the bosons interact not only via the short-range s-wave but also the long-range dipole-dipole interaction, and the dipolar interaction constitutes an additional control knob inaccessible to a nondipolar condensate and may thus open up new possibilities for engineering quantum gases with novel properties.

Motivated by this new prospect, we consider a dipolar Bose-Fermi mixture loaded in a quasi two-dimensional (2D) trap, forming a square optical lattice, where a two-component Fermi gas [Fig. 1(b)] is mixed with a single-component dipolar BEC [Fig. 1(a)]. A plethora of interesting phenomena have been predicted to occur in Bose-Fermi mixtures in square lattices, including quantum phases of composite particles involving pairing of fermions with boson particles or boson holes [34], superfluid-Mott insulator and metal-insulator transition [35] and coexistent phases [36] within a slave-rotor mean-field approximation, competition between phase separation and supersolid states driven by a combination of van Hove instabilities and Fermi surface nesting [37–39], superfluid pairings [40] and superfluid-Mott insulator transition [41] in the presence of artificial staggered magnetic field, and an interplay between density waves and superfluids with unconventional pairing symmetries based on both a mean-field study [8] and functional renormalization group analysis [42–44]. However, thus far these studies have considered nondipolar bosons that interact only through the repulsive hard-core potentials.

The focus of the present work is on the last topic — competition between density waves and unconventional superfluids, which are the cold atom analogs of the unconventional superconductors in electron systems. Conventional superconductors consist of spin-singlet s-wave BCS pairs [45] where both spin and orbital angular momenta vanish, and it has been well established that the conventional (low-T_c) superconductors are those where the pairing mechanism is dominated by the phonon-induced electron-electron interaction. The study of unconventional pairing states, where the gap parameters possess symmetries different from the usual s-wave symmetry, began with the work by Anderson and Moral [46] and that by Balian and Werthamer [47], which led to the discovery of A- and B-phase with p-wave symmetries in superfluid ^{3}He [48]. It has remained to this day an active area of research, in large part, because of the discovery of high-T_c superconductors in cuprate compounds by Bednorz and Müller in 1986 [49], which are believed to possess unconventional order parameters with $d_{x^2-y^2}$-wave symmetry [50, 51].

In this paper, for simplicity, we shall restrict our attention to superfluids where the spatial symmetry of a BCS pair can be classified according to the irreducible representations of D_4, the point group of a square. An important early work by Micnas *et al.* [52, 53] investigated, within mean-field theory, superconducting phases of the same point group, based on an extended Hubbard model with on-site repulsive and intersite attractive interactions. It was shown explicitly that when the intersite interaction is restricted to nearest neighbors, symmetrized two-body interactions in momentum space can be cast into separable forms that support parings with s-, $d_{x^2-y^2}$- and p-wave symmetries but not d_{xy}-and g-wave symmetries. In a Bose-Fermi mixture, however, the effective Fermi-Fermi interaction, which is mediated by the phonons of a BEC, has an interaction range that depends on, among other things, the effective healing length. This healing length is tunable by changing, e.g., the boson hopping amplitude. In principle, as the healing length increases, the effective Fermi-Fermi interaction may reach over many lattice sites [43]. Thus, classification by Micnas *et al.* [52] holds only in the limit where the healing length is much smaller than the lattice constant, which is precisely the argument used by Bukov and Pollet in their recent work [54] to limit superfluids to those with s-, $d_{x^2-y^2}$-, and p-wave symmetries. In contrast, we do not place such a constraint on our model and we therefore include superfluids with d_{xy}- and g-wave symmetries, which cannot be excluded a priori in the presence of a long-range interaction [55]. The inclusion of these two phases allows us to take into consideration a wider choice of possibilities when analyzing phase diagrams, making our studies, to some extent, more rigorous than those without them.

This paper is organized as follows. In Sec. II, we introduce a set of 2D two-body interactions including onsite and offsite (nearest-neighbors) dipolar ones, reducing our 3D trap model to a quasi 2D system in a square optical lattice and describe it with the single-band Bose-Fermi Hamiltonian in both real and reciprocal lattice space.

In Sec. III, we introduce phonons that obey the dispersion spectra of a homogeneous dipolar BEC. In the same section, we eliminate the phonon degrees of freedom and arrive at an effective Hamiltonian where fermions interact not only with the hard-core potential but also the phonon-induced interaction.

In Sec. IV, we take the Hartree-Fock Bogoliubov mean-field approach and construct, in the space spanned by the base functions of the irreducible representations of D_4, the matrix representation of the linearized gap equation. The main complexity in this endeavor comes from evaluating the related matrix elements which are 4D integrals in momentum space involving symmetrized interactions that depend on momenta in a nontrivial way, something absent in the simplest BCS theory. The gap equation in the simplest BCS theory (for the s-wave superfluid pairing in continuous 3D models) can be reduced to Eq. (64) involving a 1D integral, which is the origin of the well-known formula, Eq. (65), that one uses to estimate the

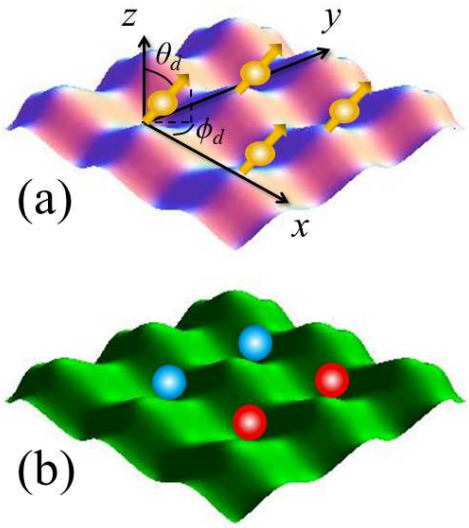

FIG. 1. (Color online) A dipolar condensate (a) is mixed with a two-component nondipolar Fermi gas (b) to form a dipolar Bose-Fermi mixture in a 2D square optical lattice. All dipoles are pinned, by an external field, to (θ_d, ϕ_d), which are respectively the polar and azimuthal coordinates defined relative to the 2D optical lattice.

critical temperature. A major contribution of the present work is that by using a combination of algebra involving elliptical integrals and symmetry considerations, we are able to reduce the 4D integrals in our model into 1D integrals. This reduction results in a set of 1D integral equations analogous to Eq. (64) for all the possible superfluid phases classified under the irreducible representations of group D_4. An example derivation is given in the Appendix to highlight the main techniques we employed to achieve such simplifications.

In Sec. V, we derive the conditions for the onset of the spin-density and charge-density waves, two possible orderings arising from the instability of the Fermi gas against the density-density fluctuation.

In Sec. VI, we apply the formulas that we developed in Sec. IV and V and perform a detailed investigation of the effect that various system parameters (e.g. the healing length, the Fermi filling factor, and the dipolar interaction) have on the critical temperatures for the onset of various competing orders.

Finally, in Sec. VII, we summarize the results and highlight the significance of our work.

2. Model and Hamiltonians for the Dipolar Bose-Fermi Mixture

Let us now describe our model in some detail. The mixture under consideration consists of a single-component BEC made up of dipolar bosons of mass m_b [Fig. 1(a)] and a two-component Fermi gas made up of spin up $\uparrow$ and spin down $\downarrow$ (nondipolar) fermions of mass m_f with population balance [Fig. 1(b)] in square optical lattices. An external field is introduced to align all dipoles along its direction $\hat{\mathbf{e}}$, a unit vector specified by elevation and azimuthal angles, (θ_d, ϕ_d), which are defined with respect to the 2D lattice plane as illustrated in Fig. 1. The system is assumed to operate in the quasi-2D regime where atoms still experience 3D interactions which are divided into a short- and long-range part. The short-range part is made up of the s-wave scatterings characterized with the strength $U_{bb}^{3D} = 4\pi\hbar^2 a_{bb}/m_b$, between two bosons, $U_{bf}^{3D} = 4\pi\hbar^2 a_{bf}/\left[m_{bf} = 2m_b m_f/\left(m_b + m_f\right)\right]$, between a boson and a fermion, and $U_{ff}^{3D} = 4\pi\hbar^2 a_{ff}/m_F$, between two fermions of opposite spin, where $a_{\alpha\beta}$ are the relevant s-wave scattering lengths. (The s-wave interaction between two fermions of identical spins is prohibited by the Pauli exclusion principle.) The long-range part is the dipole-dipole interaction between bosons, which takes the form $U_{dd}^{3D}(\mathbf{r}) = d^2[1 - 3(\hat{\mathbf{e}} \cdot \hat{\mathbf{r}})^2]/\left|\mathbf{r}\right|^3$ in position $\mathbf{r}$ space, with d the induced dipole moment.

The quasi-2D optical lattice is created by three pairs of laser fields of wavelength λ propagating along three orthogonal directions [56, 57] where for simplicity we have assumed that the laser fields for bosons have the same wavelength as those for fermions. This arrangement creates a trap potential, $V_\alpha(\mathbf{r}) = V_{1\alpha}(z) + V_{2\alpha}(\mathbf{r}_\perp)$, for bosons $(\alpha = b)$ and fermions $(\alpha = f)$, where

$$V_{1\alpha}(z) = V_{\alpha z}\sin^2(\pi z/a), \tag{1}$$

$$V_{2\alpha}(\mathbf{r}_\perp) = V_{\alpha\perp}\left[\sin^2(\pi x/a) + \sin^2(\pi y/a)\right]. \tag{2}$$

$V_{1\alpha}(z)$ in Eq. (1), with $V_{\alpha z}$ being much stronger than $V_{\alpha\perp}$, is to provide atoms with a tight confinement along the axial dimension z while $V_{2\alpha}(\mathbf{r}_\perp)$ in Eq. (2) is to provide atoms with a qausi-2D square lattice of lattice constant $a = \lambda/2$ in the radial or transverse dimensions $\mathbf{r}_\perp = (x, y)$. The parameters are chosen in such a way that $V_{\alpha\perp}$, while much weaker than $V_{\alpha z}$, is sufficiently high compared with the photon recoil energy, $E_\alpha = 2\hbar^2\pi^2/\lambda^2 m_\alpha$, and all other energy scales are sufficiently small compared with the energy band gap (in the order of $V_{\alpha\perp}$). As such, atoms reside essentially in the lowest Bloch band and the tight binding remains a fairly good approximation. In our calculation, we assume that the single-particle Wannier functions located at site i are in a separable form, $w_\alpha(z)\, w_\alpha(\mathbf{r}_\perp)$, where

$$w_\alpha(z) = \exp\left(-z^2/2d_{\alpha z}^2\right)/\sqrt{\sqrt{\pi}d_{\alpha z}}, \tag{3}$$

$$w_\alpha(\mathbf{r}_\perp) = \exp\left(-\mathbf{r}_\perp^2 2d_{\alpha\perp}^2\right)/\sqrt{\pi}d_{\alpha\perp}, \tag{4}$$

are the ground state wavefunctions of the harmonic oscillators, with $d_{\alpha z,\perp} = \sqrt{\hbar/m_\alpha\omega_{\alpha z,\perp}}$ the harmonic oscillator lengths and $\omega_{\alpha z,\perp} = 2\sqrt{E_\alpha V_{\alpha z,\perp}}/\hbar$ the harmonic oscillator frequencies. The Bose-Fermi mixture under these approximations is described by the single-band

Bose-Fermi Hamiltonian,

$$\hat{H} = -\sum_{\langle ij\rangle}\left[t_b\hat{b}_i^\dagger\hat{b}_j + t_f\left(\hat{a}_{i,\uparrow}^\dagger\hat{a}_{j,\uparrow} + \hat{a}_{i,\downarrow}^\dagger\hat{a}_{j,\downarrow}\right) - \frac{U_{ij}}{2}\hat{n}_{i,b}\hat{n}_{j,b}\right] + \sum_i\left[\frac{U_b}{2}\hat{n}_{i,b}\left(\hat{n}_{i,b}-1\right) + U_{bf}\hat{n}_{i,b}\hat{n}_{i,f} + U_{ff}\hat{n}_{i,\uparrow}\hat{n}_{i,\downarrow}\right] - \sum_i\left[\mu_b\hat{b}_i^\dagger\hat{b}_i + \mu_f\left(\hat{a}_{i,\uparrow}^\dagger\hat{a}_{i,\uparrow} + \hat{a}_{i,\downarrow}^\dagger\hat{a}_{i,\downarrow}\right)\right], \quad (5)$$

where $\langle ij\rangle$ stands for the summation over nearest neighbors, $\hat{b}_i$ and $\hat{a}_{i,\sigma}$ are the field operators for bosons and fermions of spin $\sigma\,(=\uparrow,\downarrow)$ at site i, respectively, $\hat{n}_{i,b} = \hat{b}_i^\dagger\hat{b}_i$ and $\hat{n}_{i,\sigma} = \hat{a}_{i,\sigma}^\dagger\hat{a}_{i,\sigma}$ $(\hat{n}_{i,f} = \hat{n}_{i,\uparrow} + \hat{n}_{i,\downarrow})$ are the corresponding particle number operators, and μ_b and μ_f are the chemical potentials for bosons and fermions, respectively. The Hamiltonian (5) has been expressed in terms of various effective 2D coefficients whose explicit expressions we now present. The kinetic energy part of the Hamiltonian is described by the terms proportional to the hopping amplitudes between nearest neighbors [38, 58, 59]

$$t_\alpha \simeq \frac{4}{\sqrt{\pi}}E_\alpha\left(\frac{V_{\alpha\perp}}{E_\alpha}\right)^{3/4}\exp\left(-2\sqrt{\frac{V_{\alpha\perp}}{E_\alpha}}\right). \quad (6)$$

The on-site interactions consist of

$$U_{ff} = U_{ff}^{3D}\left(\sqrt{2\pi}d_{fz}\right)^{-1}\left(2\pi d_{f\perp}^2\right)^{-1}, \quad (7)$$

$$U_{bf} = U_{bf}^{3D}\left(\sqrt{\pi\left(d_{bz}^2 + d_{fz}^2\right)}\right)^{-1}\left[\pi\left(d_{b\perp}^2 + d_{f\perp}^2\right)\right]^{-1}, \quad (8)$$

$$U_{bb} = U_{bb}^{3D}\left(\sqrt{2\pi}d_{bz}\right)^{-1}\left(2\pi d_{b\perp}^2\right)^{-1}, \quad (9)$$

which are 2D analogs of 3D short-range s-wave interactions, $U_{\alpha\beta}^{3D}$, introduced in the beginning of the section. As to the long-range dipole-dipole interaction, it contributes both to the onsite interaction and the off-site interaction. The former is given by [33]

$$U_{dd} = 2U_{bb}\times\left[\chi_{dd}\equiv\varepsilon_{dd}\left(1-\frac{3}{2}\sin^2\theta_d\right)\zeta\right], \quad (10)$$

where $\varepsilon_{dd} = 4\pi d^2/\left(3U_{bb}^{3D}\right)$ measures the dipolar interaction relative to the s-wave boson-boson interaction, and

$$\zeta = 1 + \frac{3}{2s^2}\left(1 - \frac{s^2+1}{s}\tan^{-1}s\right), \quad (11)$$

is a unitless factor fixed purely by the geometry of the trapping potential, where $s = \sqrt{\sqrt{V_{bz}/V_{b\perp}} - 1}$. The first term in the second line of Eq. (5) contains

$$U_b = U_{bb} + U_{dd} = U_{bb}\left(1 + 2\chi_{dd}\right), \quad (12)$$

which represents the total onsite interaction for bosons. Here, the use of the single-subscripted b on U_b is to stress that U_b has contributions not only from the short-range s-wave interaction U_{bb} but also from the on-site dipole-dipole interaction U_{dd}. The off-site dipole-dipole interaction, owing to their rapid decay with distance $(1/r^3)$, is assumed to be limited to the nearest-neighbor (NN) dipole-dipole interaction [60], well approximated by the formula [61] $U_{ij} = d^2\left(1-3\cos^2\theta_{ij}\right)/a^3$, where θ_{ij} is the angle between the dipole and the displacement from site i to nearest site j.

To study the superfluid pairings, we move to the lattice momentum space (with a total of N_L sites) in which $\hat{b}_{\mathbf{k}}$ and $\hat{a}_{\mathbf{k},\sigma}$ are field operators and $\hat{\rho}_{\mathbf{k},b} = \sum_{\mathbf{q}}\hat{b}_{\mathbf{q}+\mathbf{k}}^\dagger\hat{b}_{\mathbf{q}}$ and $\hat{\rho}_{\mathbf{k},\sigma} = \sum_{\mathbf{q}}\hat{a}_{\mathbf{q}+\mathbf{k},\sigma}^\dagger\hat{a}_{\mathbf{q},\sigma}$ $(\hat{\rho}_{\mathbf{k},f} = \hat{\rho}_{\mathbf{k},\uparrow} + \hat{\rho}_{\mathbf{k},\downarrow})$ are the corresponding particle number operators, and transform the Hamiltonian in Eq. (5) into

$$\hat{H} = \sum_{\mathbf{k}}\left(\epsilon_{\mathbf{k},b} - \mu_b\right)\hat{b}_{\mathbf{k}}^\dagger\hat{b}_{\mathbf{k}} + \frac{1}{2N_L}\sum_{\mathbf{k}}\left[U_b + 2U\left(\mathbf{k}\right)\right]\hat{\rho}_{\mathbf{k},b}\hat{\rho}_{-\mathbf{k},b} + \sum_{\mathbf{k}\sigma}\left(\epsilon_{\mathbf{k},f} - \mu_f\right)\hat{a}_{\mathbf{k},\sigma}^\dagger\hat{a}_{\mathbf{k},\sigma} + \frac{1}{N_L}\sum_{\mathbf{k}}\left(U_{bf}\hat{\rho}_{\mathbf{k},b}\hat{\rho}_{-\mathbf{k},f} + U_{ff}\hat{\rho}_{\mathbf{k},\uparrow}\hat{\rho}_{-\mathbf{k},\downarrow}\right), \quad (13)$$

where the sum over the momentum $\mathbf{k}$ (or $\hbar\mathbf{k}$ to be precise) is limited to the first Brillouin zone,

$$\epsilon_{\mathbf{k},\alpha} = -2t_\alpha\left(\cos k_x + \cos k_y\right) \quad (14)$$

is the single-particle dispersion and

$$U\left(\mathbf{k}\right) = U_x\cos k_x + U_y\cos k_y \quad (15)$$

is the NN dipole-dipole interaction in momentum space, with U_x and U_y being given by

$$U_x = \frac{d^2}{a^3}\left[1 - 3\sin^2\theta_d\cos^2\phi_d\right], \quad (16)$$

$$U_y = \frac{d^2}{a^3}\left[1 - 3\sin^2\theta_d\sin^2\phi_d\right]. \quad (17)$$

We have used the unit convention in which k_x and k_y are scaled to the inverse lattice constant $1/a$.

3. Phonons and Effective Fermi Hamiltonian

An ultracold Bose gas can be prepared in ground states of rather different natures, e.g., superfluid and Mott insulator phases, depending on the filling factor and strength of the two-body particle interaction relative to the hopping energy. A number of papers studied Bose-Fermi mixtures in which the Bose gas operates in the parameter regime close to the Mott insulator-superfluid transition with a relatively low boson filling factor (see, e.g.,

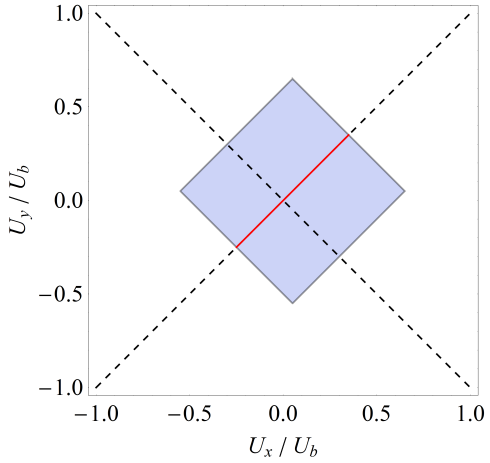

FIG. 2. (Color online) The shaded region in the (U_x,U_y) plane for $t_b/n_bU_b = 1$ supports a stable homogeneous dipolar BEC. For a system where the NN interaction is isotropic, such a uniform superfluid exists only along the solid red diagonal line.

references [36, 62]). A dipolar Bose gas is more complex than its nondipolar counterpart and thus may enter additional phases. In our model here, owing to the dipoles being directed away from the axial direction, the dipole-dipole interaction inherits both side-by-side repulsion and head-to-tail attraction. This, along with the ability to tune the ratios n_bU_b/t_b and U_x/U_y, makes not only the superfluid and Mott insulator but also supersolid phases accessible to the present 2D dipolar system. We focus on the Bose-Fermi mixture in which the Bose gas operates in the superfluid region where the dipolar superfluid phase is characterized with a uniform order parameter $\langle \hat{b}_j \rangle = \sqrt{n_b}$, a chemical potential $\mu_b = -4t_b + n_b(U_b + 2U(0))$, and a Bogoliubov excitation spectrum

$$E_{\mathbf{k},b} = \sqrt{(\epsilon_{\mathbf{k},b} + 4t_b)\left(\epsilon_{\mathbf{k},b} + 4t_b + 2n_b\left[U_b + 2U\left(\mathbf{k}\right)\right]\right)}, \tag{18}$$

where $U(\mathbf{k})$ has been defined in Eq. (15). This superfluid phase exists in the parameter space where $E_{\mathbf{k},b}$ is real; when $E_{\mathbf{k},b}$ changes from real to imaginary, the dipolar gas may undergo a dynamical instability towards other competing phases. The parameter region that supports a stable homogeneous superfluid in the (U_x, U_y) space is marked in Fig. 2 as a square bordered by the four lines $2U_x+2U_y+U_b = 0$, $2U_x+2U_y-U_b-4t_b/n_b = 0$, $2U_x-2U_y-U_b-2t_b/n_b = 0$, and $2U_y-2U_x-U_b-2t_b/n_b = 0$. Inside the square, the excitation spectra in the long wavelength limit, at the mode of the checkerboard supersolid phase $\mathbf{k} = (\pi/a, \pi/a)$, and at the modes of the striped supersolid phase $\mathbf{k} = (\pi/a, 0)$ and $(0, \pi/a)$, are all real [63].

As is well-known, in a Bose-Fermi mixture, phonons of the condensate can induce an effective attraction between two fermions [6]. As a result, in addition to interacting through the s-wave interaction (between fermions of opposite spins) with strength U_{ff}, two fermions can interact indirectly by exchanging virtual phonons. Exchanging virtual phonons in this fashion induces between two fermions an effective spin-independent attractive interaction, which, in momentum space, is given by

$$U_{ind}\left(\mathbf{q}\right) = -\frac{U_0\left(\equiv U_{bf}^2/U_{bb}\right)}{1 + 2\chi_{dd} + \xi^2\left[4 - 2D\left(\mathbf{k}\right)\right]}, \tag{19}$$

where $D(\mathbf{k}) = \sum_{\alpha=x,y}(1 - 2n_bU_\alpha/t_b)\cos k_\alpha$ and $\xi = \sqrt{t_b/2n_bU_{bb}}$ is the healing length (in the unit of lattice constant a) of the bosons interacting only under the short-range s-wave interaction. In arriving at Eq. (19), we have ignored the retardation effect. This implies that Eq. (19) holds when the characteristic energy scale of fermions is small in comparison to that of phonons, which translates into the fast phonon limit. In this limit, the phonon velocity is much larger than the Fermi velocity so that the phonon degrees of freedom can be adiabatically eliminated, leading to Eq. (19). However, the same formula is often used in studies where the fast phonon limit is not quite fulfilled. The rational behind this is that the retardation effect affects the pre-exponential factor from the Fermi energy scale to some characteristic bosonic frequency scale [5, 8]. Thus, we expect it to be true for our dipolar Bose-Fermi mixture as well—including the retardation effect will not affect the (qualitative) predictive power of the formulas we aim to derive in this work.

The effective Hamiltonian for fermions after integrating out the phonon degrees of freedom becomes, apart from a c-number,

$$\begin{aligned}\hat{H}_F = &\sum_{\mathbf{k},\sigma}\left(\epsilon_{\mathbf{k},f} - \mu_f + n_bU_{bf}\right)\hat{a}^\dagger_{\mathbf{k},\sigma}\hat{a}_{\mathbf{k},\sigma} \\ &+ \frac{1}{2N_L}\sum_{\mathbf{q},\sigma,\sigma'}U_{\sigma,\sigma'}\left(\mathbf{q}\right)\hat{\rho}_{\mathbf{q},\sigma}\hat{\rho}_{-\mathbf{q},\sigma'},\end{aligned} \tag{20}$$

where

$$U_{\sigma,\sigma'}\left(\mathbf{q}\right) = U_{ff}\delta_{\sigma',-\sigma} + U_{ind}\left(\mathbf{q}\right) \tag{21}$$

is the total effective Fermi-Fermi interaction. We shall make two important comments concerning our assumptions in arriving at this effective Hamiltonian.

First, we have taken into account only the effect of bosons on fermions in the form of the phonon-mediated interaction. In the presence of Bose-Fermi interaction, fermions will always disturb and therefore modify the Bose gas. This will result in a correction to the Bose gas proportional to the Bose-Fermi interaction. This correction will, in turn, affect the Fermi gas, which, in terms of the Bose-Fermi interaction, is a higher order effect than the effect of the undisturbed Bose gas on the Fermi gas. Therefore, one can ignore the former effect in comparison to the latter one in the limit of weak Bose-Fermi interaction.

Second, we have neglected the fermion-induced interaction, in which a fermion interacts with a second fermion via polarization of the fermionic background by the second fermion. Gor'kov and Melik-Barkhudarov [64] found this interaction to be responsible for an order unity correction to the critical temperature of the superfluid with s-wave symmetry in Fermi gases with bare attractive interactions (also see [65]). The same induced-interaction was proposed by Kohn and Luttinger [66] as a pairing mechanism (Kohn-Luttinger mechanism) for realizing superfluids with high-partial wave symmetries in Fermi gases with bare repulsive interactions. As such, this induced interaction plays an important role in the exploration of pairing physics in pure Fermi gases. In a Bose-Fermi mixture, however, not only background fermions but also phonons of the BEC can mediate an interaction between fermions. The former interaction can be ignored in situations where it is much weaker than the latter interaction [67], which will be our case here. Additionally, we may ignore the fermion interaction since the Kohn-Luttinger effect in 2D systems with rotational invariance is exponentially suppressed compared with its 3D counterpart [68], and our model takes place in the setting of a 2D lattice. At any rate, our results in this paper, like those in many others (see, for example, [7, 8, 54]) which also ignore the Kohn-Luttinger mechanism, hold in the parameter space where the phonon-induced interaction dominates.

4. Superfluid States

At temperatures below the Fermi temperature, fermions tend to form the normal ground state (Fermi sea), in which states below the Fermi energy are all occupied with each state accommodating one particle. As in crystal solids, the phonon-mediated interaction in our model, being attractive, may serve as a catalyst, causing the normal state to undergo dynamical instability towards the BCS state, in which fermions are divided into highly correlated pairs with opposite momenta. This normal-to-superfluid phase-transition is accompanied with a lowering of symmetry and is therefore of second-order in nature. It is characterized by a symmetry-breaking order parameter, known as the gap, that represents the extent of macroscopic phase coherence.

To study the BCS state of a fermionic system described by the effective Hamiltonian (20), we use the self-consistent Hartree-Fock-Bogoliubov mean-field approach [69], in which we associate the BCS paring with the gap parameter $\Delta_{\sigma,\sigma'}(\mathbf{k}) = \sum_{\mathbf{q}} U_{\sigma,\sigma'}(\mathbf{k}-\mathbf{q}) \langle \hat{a}_{-\mathbf{q},\sigma} \hat{a}_{\mathbf{q},\sigma'} \rangle / N_L$, direct pairing with the Hartree potential $\Sigma^{'} = \sum_{\sigma'} U_{\sigma,\sigma'}(0) n_{\sigma'}$, and exchange paring with the Fock potential $\Sigma(\mathbf{k}) = -\sum_{\mathbf{q}} U_{ind}(\mathbf{k}-\mathbf{q}) \langle \hat{a}^{\dagger}_{\mathbf{q},\sigma} \hat{a}_{\mathbf{q},\sigma} \rangle / N_L$. A further application of the Bogoliubov diagonalization procedure leads to the gap equation

$$\Delta_{\sigma,\sigma'}(\mathbf{k}) = -\sum_{\mathbf{q}} \frac{U_{\sigma,\sigma'}(\mathbf{k}-\mathbf{q})}{N_L} \frac{\tanh \frac{E_{\mathbf{q}}}{2T}}{2E_{\mathbf{q}}} \Delta_{\sigma,\sigma'}(\mathbf{q}), \quad (22)$$

and the particle number equation

$$n_f = \frac{1}{N_L} \sum_{\mathbf{q}} \left(1 - \frac{\xi'_{\mathbf{q}}}{E_{\mathbf{q}}} \tanh \frac{E_{\mathbf{q}}}{2T} \right), \quad (23)$$

where $\xi'_{\mathbf{k}} = (\xi_{\mathbf{k}} \equiv \epsilon_{\mathbf{k},f} - \mu_f) + \Sigma(\mathbf{k})$, and $E_{\mathbf{k}} = \sqrt{\xi'^2_{\mathbf{k}} + \Delta^2_{\sigma,\sigma'}(\mathbf{k})}$ is the fermionic quasi-particle spectrum. In Eq. (22), we have adjusted the chemical potential according to $\mu_f \rightarrow \mu_f - [U_{bf} n_b + U_{ind}(0) n_f + U_{ff} n_f/2]$, where $n_f = n_\uparrow + n_\downarrow$ is the total density of fermions, which is also known as the fermion filling factor. Note that in this paper, we absorb the Boltzmann constant k_B into the temperature T so that T has the units of energy.

The gap parameter $\Delta_{\sigma,\sigma'}(\mathbf{q})$ in Eq. (22), according to the Landau theory of second order phase transitions [70], must transform according to one of the irreducible representations of the symmetry group of the high-temperature disordered phase. The symmetry group to which the effective Hamiltonian $\hat{H}_F$ in Eq. (20) belongs is dictated, in our model where the hopping is assumed to be isotropic, by the symmetry underlying the Fermi-Fermi interaction. In this work, we explore the superfluid phases of the effective Hamiltonian $\hat{H}_F$ [Eq. (20)] that preserves the symmetry of a square lattice. Hence, we limit our study to systems that operate, within the (shaded) region in the (U_x, U_y) space of Fig. 2, along the $+45^{\circ}$(red) line, where $U_x = U_y$ and the NN interaction is isotropic. This can be achieved by fixing the azimuthal angle of the dipole to $\phi_d = 45^{\circ}$ while changing either the elevation angle θ_d or the induced dipole moment d. For such systems, the phonon-mediated Fermi-Fermi interaction, Eq. (19), simplifies to

$$U_{ind}(\mathbf{k}) = -\frac{U_0}{1 + 2\chi_{dd} + \xi^2 [4 - b\gamma_{\mathbf{k}}]}, \quad (24)$$

where

$$b = 1 - \frac{1}{2} \frac{\chi_{dd}}{\xi^2} \times \left[G \equiv \frac{3}{2} \frac{U^{3D}_{bb}}{U_{bb}} \frac{1}{\pi a^3 \zeta} \right], \quad (25)$$

and

$$\gamma_{\mathbf{k}} = 2(\cos k_x + \cos k_y). \quad (26)$$

The table in Fig. 3 lists the irreducible representations of the point group D_4 along with the simplest possible base functions (for a square lattice) that transform according to the corresponding representations [66]. We stress that for each irreducible representation, there corresponds infinitely many other base functions. However, near the Fermi surface, the quasiparticle energy is determined by

Rep.	Base Function	Symmetry
A_1	$1, \cos k_x + \cos k_y$	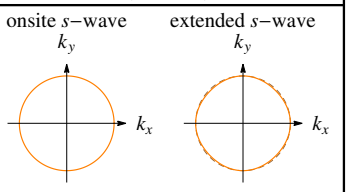
A_2	$\sin k_x \sin k_y \times (\cos k_x - \cos k_y)$	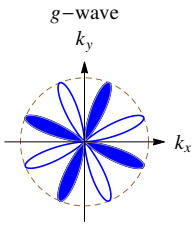
B_1	$\cos k_x - \cos k_y$	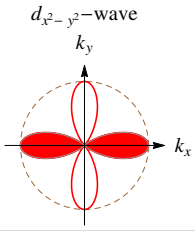
B_2	$\sin k_x \sin k_y$	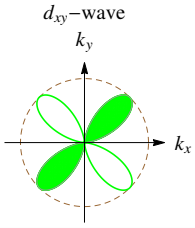
E	$\{\sin k_x, \sin k_y\}$	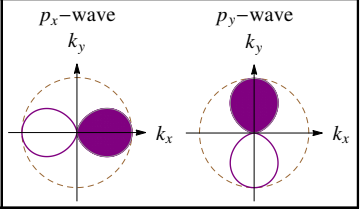

FIG. 3. (Color online) The irreducible representations of symmetry group D_4 along with their base functions.

the gap parameter (which is a function of k). It is thus energetically favorable for the gap parameter to have as few nodes as possible on the Fermi surface, suggesting that the pairing phases that will most likely materialize are those with the simplest possible base functions [71, 72]. This may explain why well-known works (see, for example, review articles [50] and [51]) use the simplest base functions listed in Fig. 3 to classify superfluid order parameters.

As can be seen, the function $\gamma_{\mathbf{k}}$ in Eq. (24) transforms according to the total symmetric representation, A_1. Hence, as anticipated, the interaction in Eq. (24) exhibits the same symmetry as that of the underlying optical lattice which, for a square lattice, is described by the point group D_4.

In the spirit of the Landau theory of second-order phase transitions, we now expand the gap parameter in the space spanned by the base functions of the point group D_4 in Fig. 3,

$$\begin{aligned}\Delta_{\sigma,\sigma'}(\mathbf{k}) = {} & \delta_{\sigma,-\sigma'}\left(\Delta_{s0} + \Delta_{s1}\gamma_{\mathbf{k}} + \Delta_{d_{x^2-y^2}}\eta_{\mathbf{k}}\right) \\ & + \delta_{\sigma,-\sigma'}\left(\Delta_{d_{xy}}\beta_{\mathbf{k}} + \Delta_g\beta_{\mathbf{k}}\eta_{\mathbf{k}}\right) \\ & + \delta_{\sigma,\sigma'}\left(\Delta_{px}\sin k_x + \Delta_{py}\sin k_y\right), \end{aligned} \tag{27}$$

where $\gamma_{\mathbf{k}}$ has been defined previously in Eq. (26) and

$$\eta_{\mathbf{k}} = 2\left(\cos k_x - \cos k_y\right), \quad \beta_{\mathbf{k}} = \sin k_x \sin k_y. \tag{28}$$

The gap parameter behaves very much like the wave function for two identical fermions. It is made up of two parts: a spin part and a spatial part. The first two lines in Eq. (27) are devoted to the superfluids in the spin singlet sector where the spin part is in the singlet state antisymmetric with respect to spin exchange and the spatial part must then transform according to the four parity-odd 1D representations $A_{1,2}$ and $B_{1,2}$ in order to meet the Fermi statistics. In contrast, the last line in Eq. (27) is devoted to the superfluids in the spin triplet sector where the spin part is in the triplet state symmetric with respect to spin exchange and the spatial part must then transform according to the parity-even 2D representation E. Accordingly, Δ_{s0}, Δ_{s1}, $\Delta_{d_{x^2-y^2}}$, $\Delta_{d_{xy}}$ and Δ_g in Eq. (27) are the gap parameters for the superfluids in the spin singlet sector with on-site s-, extended s-, $d_{x^2-y^2}$-, d_{xy}-, and g-wave symmetries, respectively, while Δ_{px} and Δ_{py} in Eq. (27) are the gap parameters for the superfluids in the spin triplet sector with p-wave symmetries.

The gap parameter is vanishingly small near the critical temperature. In order to determine the critical temperature for each superfluid state, we insert the ansatz (27) into the gap equation (22) linearized around $\Delta_{\sigma,\sigma'}(\mathbf{q}) = 0$ and replace $U_{\sigma,\sigma'}(\mathbf{k},\mathbf{q})$ either with the singlet potential,

$$U_s(\mathbf{k},\mathbf{q}) = U_{ff} + \frac{U_{ind}(\mathbf{k}-\mathbf{q}) + U_{ind}(\mathbf{k}+\mathbf{q})}{2}, \tag{29}$$

or with the triplet potential,

$$U_t(\mathbf{k},\mathbf{q}) = \frac{U_{ind}(\mathbf{k}-\mathbf{q}) - U_{ind}(\mathbf{k}+\mathbf{q})}{2}, \tag{30}$$

depending on whether the gap equation falls into the singlet or triplet sector of superfluid pairings. This procedure is equivalent to finding, in the space spanned by the base functions of the irreducible representations of the point group D_4, the matrix representation of the linearized gap equation, which, due to the inherent symmetry of our model, is expected to be block diagonal. For organizational purposes, we divide the gap equation in the spin singlet sector into one for the s-wave pairing,

$$\begin{pmatrix} s_0^0 - 1 & s_0^1 \\ s_1^0 & s_1^1 - 1 \end{pmatrix} \begin{pmatrix} \Delta_{s0} \\ \Delta_{s1} \end{pmatrix} = 0, \tag{31}$$

where

$$s_0^0 = -\sum_{\mathbf{k},\mathbf{q}} U_s\left(\mathbf{k},\mathbf{q}\right) S_{\mathbf{q}}\left(T\right), \tag{32a}$$

$$s_0^1 = -\sum_{\mathbf{k},\mathbf{q}} U_s\left(\mathbf{k},\mathbf{q}\right) S_{\mathbf{q}}\left(T\right) \gamma_{\mathbf{q}}, \tag{32b}$$

$$s_1^0 = -\sum_{\mathbf{k},\mathbf{q}} U_s\left(\mathbf{k},\mathbf{q}\right) S_{\mathbf{q}}\left(T\right) \frac{\gamma_{\mathbf{k}}}{4}, \tag{32c}$$

$$s_1^1 = -\sum_{\mathbf{k},\mathbf{q}} U_s\left(\mathbf{k},\mathbf{q}\right) S_{\mathbf{q}}\left(T\right) \frac{\gamma_{\mathbf{k}}\gamma_{\mathbf{q}}}{4}, \tag{32d}$$

and one for the $d_{x^2-y^2}$-, d_{xy}-, and g-wave pairings,

$$\begin{pmatrix} d_0 - 1 & 0 & 0 \\ 0 & d_1 - 1 & 0 \\ 0 & 0 & g - 1 \end{pmatrix} \begin{pmatrix} \Delta_{d_{x^2-y^2}} \\ \Delta_{d_{xy}} \\ \Delta_g \end{pmatrix} = 0, \tag{33}$$

where

$$d_0 = -\sum_{\mathbf{k},\mathbf{q}} U_s\left(\mathbf{k},\mathbf{q}\right) S_{\mathbf{q}}\left(T\right) \frac{\eta_{\mathbf{k}}\eta_{\mathbf{q}}}{4}, \tag{34a}$$

$$d_1 = -\sum_{\mathbf{k},\mathbf{q}} U_s\left(\mathbf{k},\mathbf{q}\right) S_{\mathbf{q}}\left(T\right) 4\beta_{\mathbf{k}}\beta_{\mathbf{q}}, \tag{34b}$$

$$g = -\sum_{\mathbf{k},\mathbf{q}} U_s\left(\mathbf{k},\mathbf{q}\right) S_{\mathbf{q}}\left(T\right) 2\beta_{\mathbf{k}}\eta_{\mathbf{k}}\beta_{\mathbf{q}}\eta_{\mathbf{q}}, \tag{34c}$$

with $S_{\mathbf{q}}\left(T\right)$ being defined as

$$S_{\mathbf{q}}\left(T\right) = \tanh\left(\xi'_{\mathbf{q}}/2T\right)/2\xi'_{\mathbf{q}}. \tag{35}$$

The gap equation in the spin triplet sector is also diagonalized with the form given by

$$\begin{pmatrix} p_x - 1 & 0 \\ 0 & p_y - 1 \end{pmatrix} \begin{pmatrix} \Delta_{px} \\ \Delta_{py} \end{pmatrix} = 0, \tag{36}$$

where, due to symmetry, the coefficients $p_x = p_y \equiv p$, with p being given by

$$p = -\sum_{\mathbf{k},\mathbf{q}} U_t\left(\mathbf{k},\mathbf{q}\right) S_{\mathbf{q}}\left(T\right) 2\sin k_x \sin q_x. \tag{37}$$

The coefficients in Eqs. (32), (34) and (37) are nothing but the matrix elements [of the linearized gap equation (22), or, to be more precise, the right-hand side of Eq. (22)] between various base functions of the irreducible representations of D_4. A major complication in evaluating these coefficients is that they are functions of the Fock potential $\Sigma\left(\mathbf{k}\right)$ and chemical potential μ_f, which, in principle, are themselves unknowns to be determined self-consistently. We take two measures to reduce this complexity. First, we estimate the Fock potential on the Fermi surface and absorb it into the chemical potential. Second, we compute the chemical potential from the number equation for the $T = 0$ normal Fermi gas,

$$n_f = \frac{4}{\pi^2}\int_{-1}^{\bar{\mu}_f} K\left(1 - x^2\right) dx, \tag{38}$$

where $\bar{\mu}_f = \mu_f/4t_f$ is the scaled chemical potential and $K\left(x\right)$ is the complete elliptic integral of the first kind. (All elliptical integrals in this paper follow the convention of Ref. [73].) It is to be stressed that only in the weak interacting limit where the characteristic interaction energy is much weaker than the Fermi energy (which is roughly equal to $4t_f$ when near half filling) do both approximations hold. Thus, the expressions we will show below remain quantitatively accurate only in the weak coupling regime, but, nevertheless, are expected to help us gain some qualitative insights into the superfluid pairings under more general conditions. Note that these were the same approximations Micnas and Ranninger [52] used when they needed to gain quick insights into their critical temperatures.

In spite of these assumptions, these matrix elements remain complicated integrals in 4D momentum space involving functions, $U_{s,t}\left(\mathbf{k},\mathbf{q}\right)$, $S_{\mathbf{q}}\left(T\right)$, etc., that have nontrivial dependences on momenta. Nevertheless, as the example in the Appendix illustrates, we are able to reduce each integral into a product between a 1D integral and an analytical function. The 1D integral (to be defined shortly) is with respect to $x \equiv \epsilon_{\mathbf{k},f}/4t_f$ and involves

$$S_{\pm}\left(x,\bar{T}\right) = S\left(x,\bar{T}\right) \pm S\left(-x,\bar{T}\right), \tag{39}$$

where

$$S\left(x,\bar{T}\right) = \frac{\tanh\left(\frac{x-\bar{\mu}_f}{2\bar{T}}\right)}{2\left(x-\bar{\mu}_f\right)}, \tag{40}$$

is $S_{\mathbf{q}}\left(T\right)$ of Eq. (35) in the scaled form. The analytical function will be one of the following functions:

$$I_1 = \frac{1}{\pi^3}\left[\frac{\bar{U}_0\chi}{b\xi^2}K\left(\chi^2\right) - 2\pi\bar{U}_{ff}\right], \tag{41a}$$

$$I_2 = \frac{\bar{U}_0\left[K\left(\chi^2\right) - \frac{\pi}{2}\right]}{\pi^3 b\xi^2}, \tag{41b}$$

$$I_3 = \frac{8}{3\pi^3}\frac{\bar{U}_0}{b\xi^2}\left[\left(\frac{4}{\chi} - 2\chi\right)K\left(\chi^2\right) - \frac{4}{\chi}E\left(\chi^2\right)\right], \tag{41c}$$

$$I_4 = \frac{32}{15\pi^3}\frac{\bar{U}_0}{b\xi^2}\left\{2\pi - \left(\frac{4}{\chi}\right)^2 E\left(\chi^2\right)\right. \tag{41d}$$

$$\left. + \left[\left(\frac{4}{\chi}\right)^2 - 12\right]K\left(\chi^2\right)\right\}, \tag{41e}$$

where $K\left(x\right)$ and $E\left(x\right)$ are, respectively, complete elliptical integrals of the first and second kind, and χ is a function defined as

$$\chi = \frac{4b\xi^2}{1 + 2\chi_{dd} + 4\xi^2}. \tag{42}$$

Here, the scaled variables, $\bar{U}_0 = U_0/4t_f$, $\bar{U}_{ff} = U_{ff}/4t_f$, $\bar{T} = T/4t_f$, are similarly defined as the scaled chemical potential $\bar{\mu}_f$ introduced in Eq. (38).

The conditions for the onset of various superfluid pairings can then be expressed in terms of various 1D integrals that we now introduce. The critical temperature is determined from

$$\det \left| \begin{array}{cc} s_0^0\left(\bar{T}\right)-1 & s_0^1\left(\bar{T}\right) \\ s_1^0\left(\bar{T}\right) & s_1^1\left(\bar{T}\right)-1 \end{array} \right| = 0, \tag{43}$$

for the pairing with the s-wave symmetry, where

$$s_0^0 = I_1 \int_0^1 K\left(1-x^2\right) S_+\left(x,\bar{T}\right) dx, \tag{44a}$$

$$s_0^1 = -I_1 \int_0^1 4xK\left(1-x^2\right) S_-\left(x,\bar{T}\right) dx, \tag{44b}$$

$$s_1^0 = -I_2 \int_0^1 xK\left(1-x^2\right) S_-\left(x,\bar{T}\right) dx, \tag{44c}$$

$$s_1^1 = I_2 \int_0^1 4x^2 K\left(1-x^2\right) S_+\left(x,\bar{T}\right) dx, \tag{44d}$$

from

$$p\left(\bar{T}\right) = 1, \tag{45}$$

for the p-wave pairing, where

$$p = I_2 \int_0^1 4\left[E\left(1-x^2\right) - x^2 K\left(1-x^2\right)\right] S_+\left(x,T\right) dx, \tag{46}$$

and finally from

$$d_0\left(\bar{T}\right) = 1, \quad d_1\left(\bar{T}\right) = 1, \quad g\left(\bar{T}\right) = 1, \tag{47}$$

for the pairings with $d_{x^2-y^2}$-, d_{xy}-, and g-wave symmetries, respectively, where

$$d_0 = I_2 \int_0^1 dx S_+\left(x,\bar{T}\right) 8\left(1+x\right)\left\{K\left[\left(\frac{1-x}{1+x}\right)^2\right] - E\left[\left(\frac{1-x}{1+x}\right)^2\right]\right\}, \tag{48}$$

$$d_1 = I_3 \int_0^1 dx S_+\left(x,\bar{T}\right)\left(1+x\right)\left\{\left(1+x^2\right)E\left[\left(\frac{1-x}{1+x}\right)^2\right] - 2xK\left[\left(\frac{1-x}{1+x}\right)^2\right]\right\}, \tag{49}$$

$$g = I_4 \int_0^1 dx S_+\left(x,\bar{T}\right)\left\{\left(1+14x^2+x^4\right)\left(1+x\right)E\left[\left(\frac{1-x}{1+x}\right)^2\right] - 2x\left(1+x\right)\left(1+6x+x^2\right)K\left[\left(\frac{1-x}{1+x}\right)^2\right]\right\}. \tag{50}$$

The reduction of 4D integrals into 1D integrals, which constitute the main results of the present work, involves an extensive use of algebra containing elliptical integrals and symmetry considerations. In the Appendix, we show how to simplify the matrix element for the d-wave pairing from Eq. (34a) into Eq. (48), using it as an example to showcase the techniques that help us simplify the matrix elements for all other pairings. The reasons why we consider these results significant will be presented in the final section (Sec. VII) where we conclude this work.

5. CDW and SDW States

The subject of fermionic superfluids studied in the previous section is founded on an instability discovered by Cooper — in the presence of an attractive interaction, irrespective of its weakness, two fermions on a Fermi surface find it energetically favorable to form a bound state, thereby causing a normal Fermi gas to undergo dynamical instability towards the BCS state. This, however, is not the only instability which a normal Fermi gas may experience. In our model, fermions are subject to the density-density interaction, $N_L^{-1}\sum_{\mathbf{k}} U_{bf}\hat{\rho}_{\mathbf{k},b}\hat{\rho}_{-\mathbf{k},f}$, due to the s-wave scattering between bosons and fermions. This interaction induces a change in the fermion density, which, within linear response theory, equals $2U_{bf}\chi\left(\mathbf{q}\right)\hat{n}_b\left(\mathbf{q}\right)$ for a two-component Fermi gas, where

$$\chi\left(\mathbf{q},T\right) = \frac{1}{N_L}\sum_{\mathbf{k}} \frac{f\left(\xi_{\mathbf{k}}\right) - f\left(\xi_{\mathbf{k}+\mathbf{q}}\right)}{\xi_{\mathbf{k}} - \xi_{\mathbf{k}+\mathbf{q}} + i\eta}, \tag{51}$$

is the well-known Lindhard function (in the static limit) with $f\left(x\right) = \left[1+\exp\left(x/T\right)\right]^{-1}$ the Fermi distribution function.

For continuous models, no drastic response of this function occurs at any $\mathbf{q}$ in 3D and 2D, but does in 1D, where it is found to diverge logarithmically at $q = Q \equiv 2k_F$. The Fermi surface of a 1D Fermi gas consists of two points, one at $+k_F$ and the other at $-k_F$. This along with the dispersion relation being linear near the Fermi points results in a perfect nesting, where the two Fermi points can be mapped to each other via the nesting condition, $\xi_{\mathbf{k}+\mathbf{Q}} = -\xi_{\mathbf{k}}$, thereby giving a divergent contribution to the Lindhard function in Eq. (51) [74].

For discrete (lattice) 2D models, owing to the reduced symmetries (relative to the continuous 2D models), sim-

ilar nesting effects can arise. In particular, nesting is known to occur at the nesting vector $\mathbf{Q}=(\pi,\pi)$ for a half-filled Fermi gas in a square lattice, leading to the divergence of $\chi(\mathbf{Q},T\to 0)$ at half filling [37, 39]. This can also be understood from the zero temperature Lindhard susceptibility, $\chi(\mathbf{Q},T=0)$, as a function of the chemical potential μ_f. Replacing $f(\xi_{\mathbf{k}})$ with $\Theta(-\xi_{\mathbf{k}})$ at $T=0$, we can simplify Eq. (51) into

$$\chi(\mathbf{Q},T=0)=\frac{1}{2t_f\pi^2}\int_{-1}^{\mu_f/4t_f}\frac{dx}{x}K\left[1-x^2\right].$$

The singularity, $1/x$, due to nesting and the van Hover singularity, $K\left(1-x^2\right)\approx\ln\left(4/|x|\right)$, in the density of states combine to yield a divergent response of the susceptibility, in the limit of half filling where $\mu_f\to 0$, according to

$$\chi(\mathbf{Q},T=0)\approx-\frac{1}{4t_f\pi^2}\left(\ln\left|\frac{16t_f}{\mu_f}\right|\right)^2.$$

This divergence implies that at very low temperatures and when operating close to half filling, a normal Fermi gas is unstable against spatially varying density perturbations and may evolve spontaneously into phases that may rival the superfluid phases studied in the previous section. We focus on two such possibilities, the spin-density wave (SDW) characterized with order parameter

$$\Delta_{SDW}=\frac{1}{2N_L}\sum_{\mathbf{k},\sigma}\sigma\left\langle\hat{c}^{\dagger}_{\mathbf{k},\sigma}\hat{c}_{\mathbf{k}+\mathbf{Q},\sigma}\right\rangle, \tag{52}$$

where the spin density varies in space with a commensurate wavevector $\mathbf{Q}$ (the case of an incommensurate wavevector is beyond the scope of this paper), and the charge-density wave (CDW) characterized with order parameter,

$$\Delta_{CDW}=\frac{1}{2N_L}\sum_{\mathbf{k},\sigma}\left\langle\hat{c}^{\dagger}_{\mathbf{k},\sigma}\hat{c}_{\mathbf{k}+\mathbf{Q},\sigma}\right\rangle, \tag{53}$$

where the charge density modulates in space with a commensurate wavevector $\mathbf{Q}$.

In the same spirit as the Hartree-Fock Bogoliubov mean-field approach that we employed previously in the study of superfluid pairings, we arrive at the mean-field equation for the order parameter Δ_{SDW}

$$1=\frac{U_{ff}}{4N_L}\sum_{\mathbf{k}}\frac{\tanh\frac{E_{\mathbf{k},+}}{2T}-\tanh\frac{E_{\mathbf{k},-}}{2T}}{\sqrt{\left(\frac{\xi'_{\mathbf{k},\uparrow}-\xi'_{\mathbf{k}+\mathbf{Q},\uparrow}}{2}\right)^2+U_{ff}^2\left|\Delta_{SDW}\right|^2}}, \tag{54}$$

and that for the particle number density

$$n_\sigma=1-\frac{1}{2N_L}\sum_{\mathbf{k}}\left(\tanh\frac{E_{\mathbf{k},+}}{2T}+\tanh\frac{E_{\mathbf{k},-}}{2T}\right), \tag{55}$$

where

$$E_{\mathbf{k},\pm}=\frac{\xi'_{\mathbf{k}}+\xi'_{\mathbf{k}+\mathbf{Q}}}{2}\pm\sqrt{\left(\frac{\xi'_{\mathbf{k}}-\xi'_{\mathbf{k}+\mathbf{Q}}}{2}\right)^2+U_{ff}^2\left|\Delta_{SDW}\right|^2}. \tag{56}$$

The same set of equations become the ones for the CDW state with the substitution of Δ_{SDW} with Δ_{CDW} and U_{ff} with $-\left[2U_{ind}(\mathbf{Q})+U_{ff}\right]$. In the weak interacting regime where one can ignore the Fock potential and fix the chemical potential according to the number equation (38) for a normal gas at $T=0$, the critical temperatures for the SDW and CDW phase are determined from the equation,

$$s\left(\bar{T}\right)=1,\quad c\left(\bar{T}\right)=1, \tag{57}$$

where

$$s=\frac{\bar{U}_{ff}}{\pi^2}\int_0^1 P\left(x,\bar{T}\right)K\left(1-x^2\right), \tag{58}$$

$$c=-\frac{2\bar{U}_{ind}(\mathbf{Q})+\bar{U}_{ff}}{\pi^2}\int_0^1 P\left(x,\bar{T}\right)K\left(1-x^2\right), \tag{59}$$

with

$$P\left(x,\bar{T}\right)=\frac{1}{x}\left(\tanh\frac{x-\bar{\mu}_f}{2\bar{T}}+\tanh\frac{x+\bar{\mu}_f}{2\bar{T}}\right), \tag{60}$$

and

$$\bar{U}_{ind}(\mathbf{Q})=-\frac{\bar{U}_0}{4\xi^2 b\left(1+\chi^{-1}\right)}, \tag{61}$$

where $\bar{U}_{ind}(\mathbf{Q})\equiv U_{ind}(\mathbf{Q})/4t_f$ is the scaled induced interaction at the nesting wavevector.

Before presenting numerical results in the next section, a comment is in order. Our results for the onset of superfluid pairings and density waves was derived within the usual mean-field approach, in which superfluid instability is treated independently from density-wave instability. A more rigorous treatment for systems operating at (or near) half filling is the parquet method [75], which couples the two instabilities. The parquet method calculates the sum of an infinite series of diagrams using flow equations from1 renormalization group theory, a system of nonlinear differential equations. In 1D near half filling, the parquet prediction is drastically different from the mean-field prediction, but in 2D near half filling the predictions qualitatively agree [76]. A quantitative comparison of the two approaches requires adapting the parquet method to our 2D model, which is beyond the scope of the current work and which we leave for future study.

6. Numerical Results and Discussions

In this section, we apply the formulas outlined in previous sections to numerically determine critical temperatures and use these results as a guide to understanding the phase structures and competing orders of the system.

6.1. Parameters

The critical temperatures depend on several parameters. Consider first $\bar{U}_{ff}$, $\bar{U}_0$, and ξ, which are functions of and thus controlled by a_{ff}, a_{bf}, and n_b. In Fig. 4, we plot (a) $\bar{U}_{ff}$ as a function of a_{ff} under different ratios of the axial to radial trap potential, and (b) $\bar{U}_0$ as a function of a_{bf} and (c) ξ as a function of n_b for different ratios of the axial to radial trap potentials as well as different ratios of the fermion to boson mass. Here and throughout what follows, we fix the wavelength to $\lambda = 1060$ nm and assume that $V_{f\perp} = V_{b\perp} \equiv V_\perp$ and $V_{fz} = V_{bz} \equiv V_z$. It is to be stressed that we do not intend to limit our investigation to particular systems in view of the rich existence of atomic elements and their isotopes in nature; the particular choices here in Fig. 4 are nothing more than to establish the orders of magnitude for the ranges in which $\bar{U}_{ff}$, $\bar{U}_0$, and ξ can vary when the corresponding control parameters are tuned within some realistic domains. As can be seen, they do not change significantly with the ratio of the axial to radial trap potential (so long as they are within the quasi-2D regime), but the healing length ξ is sensitive to the fermion-boson mass ratio and the larger this ratio, the higher the healing length.

The next parameter in line is χ_{dd}, defined in Eq. (10), a control knob inaccessible to nondipolar Bose-Fermi mixtures. As can be seen, by adjusting the polar angle of the dipole θ_d and the dipolar interaction ε_{dd}, one can change χ_{dd} continuously from positive values where the dipole is oriented close to the z axis with $\theta_d < \sin^{-1}\sqrt{2/3} = 54.7^\circ$ to negative ones where the dipole is tilted away from the z axis with $\theta_d > 54.7^\circ$. Finally, we consider G defined in Eq. (25). It can be shown that G is determined by the trap geometry according to

$$G = 6\sqrt{\frac{\pi}{2}}\frac{1}{\zeta}\frac{1}{\pi^3}\left(\frac{m_f}{m_b}\right)^{3/4}\left(\frac{E_f}{V_{bz}}\right)^{1/4}\left(\frac{E_f}{V_{b\perp}}\right)^{1/2}, \quad (62)$$

where ζ has been defined previously in Eq. (11). As can be seen from Eq. (62), G becomes small when V_{bz} and $V_{b\perp}$ become large in comparison with the photon recoil energy E_f. Thus, it is not surprising that for a quasi-2D trap where $V_{bz} \gg E_f$, G is found to be less than 1 for typical values of $V_{b\perp}$, which for our interests lie within $(3 \sim 6)\, E_f$ as illustrated in Fig. 4(d). From now on, without loss of generality, we fix G to 0.3754 for all calculations.

For systems with $G < 1$, a straightforward analysis indicates that the phonon spectrum near $\mathbf{k} = 0$ acquires an imaginary component when $\chi_{dd} < \chi_{dd}^{th} \equiv -1/[2\,(1+G)]$ and as a result, only when $\chi_{dd} > \chi_{dd}^{th}$, does the homogeneous dipolar BEC become stable against collapse. Figure 5 displays, within the first Brillouin zone, the phonon dispersion spectra for different dipolar interaction χ_{dd}. The middle surface corresponds to the spectrum without the dipolar interaction. Evident in Fig. 5 is that increasing $|\chi_{dd}|$ on the positive side (top surface) raises the phonon energy relative to the middle one. Contrarily increasing $|\chi_{dd}|$ on the negative side (bottom surface) lowers the phonon energy. This latter ability provides us with the opportunity to enhance the phonon-induced Fermi-Fermi interaction by tuning χ_{dd} on the negative side (but keeping it less than χ_{dd}^{th}).

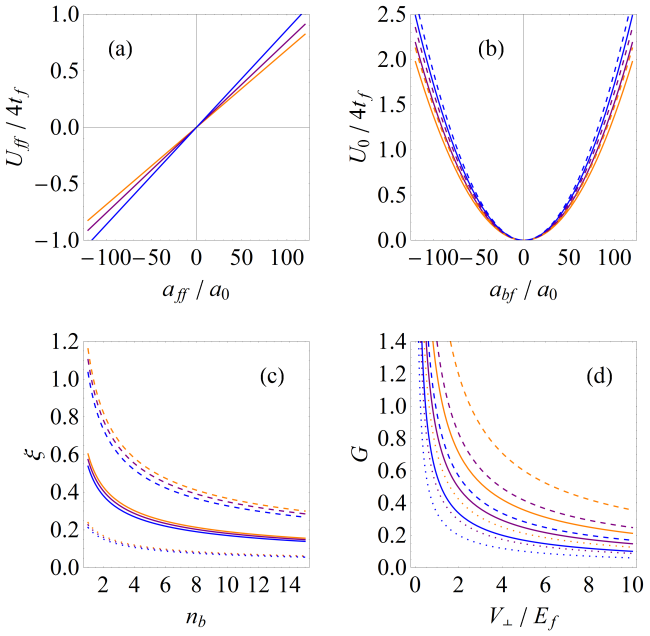

FIG. 4. (Color online) (a) $U_{ff}/4t_f$ as a function of a_{ff}, (b) $U_0/4t_f$ [defined in Eq. (19)] as a function of a_{bf}, (c) ξ as a function of n_b, and (d) G [defined in Eq. (62)] as a function of $V_\perp/E_f$. In all diagrams, $\lambda = 1060$ nm, and $V_z/V_\perp = 4$ (orange), 6 (violet), and 10 (blue). $V_\perp/E_r = 5$ in (a), (b) and (c), and $a_{bb} = 50\ a_0$ in (b) and (c), where a_0 is the Bohr radius. In (a), there exists only one group of lines because $U_{ff}/4t_f$ is mass independent. In (b), the solid curves are for $m_f/m_b = 1$ while the dashed curves are for both $m_f/m_b = 2$ and $m_f/m_b = 1/2$ because $U_0/4t_f$ is invariant with respect to the substitution $m_f/m_b \to m_b/m_f$. In (c) and (d), the solid ones are for $m_f/m_b = 1$, the dashed ones are for $m_f/m_b = 2$, and the dotted ones are for $m_f/m_b = 1/2$.

6.2. Pairing-Specific "Effective" Interactions

Having discussed the key parameters, we now seek to gain qualitative understanding of the critical temperatures as functions of these parameters. We do so from "effective" interactions which we now define. The critical temperatures are determined by matrix elements such as those in Eq. (32), each of which can be decomposed into a 1D integral, which is a function of T and μ_f (and is always positive), and a coefficient such as I_2 in Eq. (41b), which is a function of the key parameters just discussed above. This latter quantity is what we regard as the "effective" interaction strength for the corresponding phase where the symmetry of the phase has been taken into consideration. There is a total of seven phases, which

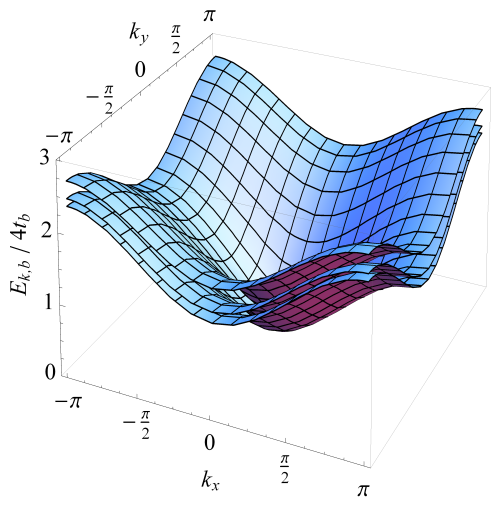

FIG. 5. (Color online) The Bogoliubov phonon spectra, $E_{\mathbf{k},b}/4t_f = \sqrt{(4-\gamma_{\mathbf{k}})\left[1+2\chi_{dd}\left(1+G\gamma_{\mathbf{k}}\right)+\xi^2\left(4-\gamma_{\mathbf{k}}\right)\right]}/4\xi$ (which is Eq. (18) for an isotropic NN interaction), for $\xi = 0.5$ and $\varepsilon_{dd} = 0.5$ (top), $\varepsilon_{dd} = 0.0$ (middle) and $\varepsilon_{dd} = -0.2$ (bottom). For all diagrams that follow in this paper, $G = 0.3754$.

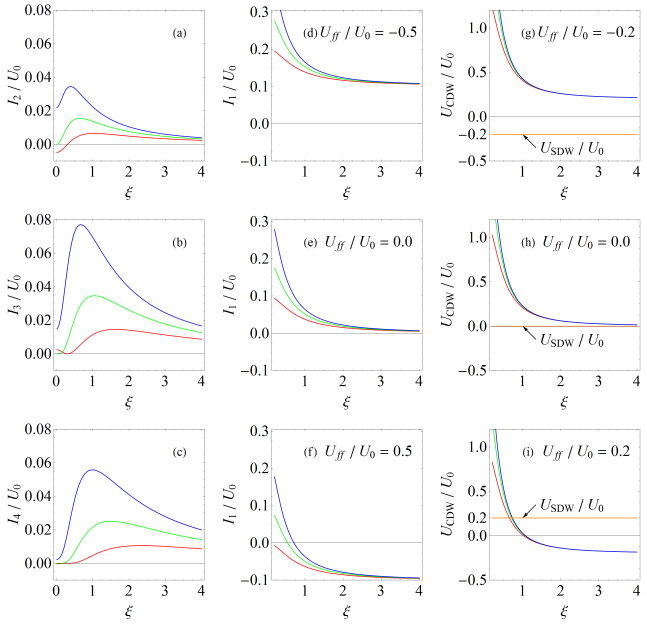

FIG. 6. (Color online) Column 1: (a) I_2/U_0 [Eq. (41b)], (b) I_3/U_0 [Eq. (41c)], and (c) I_4/U_0 [Eq. (41d)] as a function of the healing length ξ. Column 2: I_1/U_0 [Eq. (41a)] as a function of ξ when $U_{ff}/U_0 = 0.5$ (e), 0.0 (f), and -0.5 (g). Column 3: $U_{CDW}\left(\equiv -2U_{ind}(\mathbf{Q}) - U_{ff}\right)/U_0$ and $U_{CDW}\left(\equiv U_{ff}\right)/U_0$ as functions of ξ when $U_{ff}/U_0 = 0.2$ (h), 0.0 (i), and -0.2 (g). Each figure in columns 1 and 2 consists of three curves corresponding to, from *bottom* to *top*, $\varepsilon_{dd} = 0.5,\ 0$, and -0.2.

we divide into two categories. The first one consists of $d_{x^2-y^2}$-, d_{xy}-, g-, and p-wave pairing phases, whose critical temperatures are independent of U_{ff}. The second one consists of the s-wave pairing state, SDW ordering, and CDW ordering, whose critical temperatures can be either enhanced or suppressed by adjusting U_{ff}.

In the first column of Fig. 6, we plot the ratios, I_2/U_0, I_3/U_0, and I_4/U_0, which are responsible for the phases in the first category, as functions of the healing length ξ under different dipolar interactions χ_{dd}. Let us first turn our attention to the middle curve in each plot in the first column, which is produced in the absence of the dipolar interaction ($\chi_{dd} = 0$). (a) I_2, (b) I_3, and (c) I_4 reach their peak when ξ is set at 0.64, 1.04, and 1.51, respectively. This implies that in the weak coupling limit, the corresponding critical temperature is expected to reach its maximum at the corresponding peak healing length, independent of U_0. It is interesting to observe that the maximum healing length $\xi = 0.64$ for I_2, which we obtain here in a semi-analytical fashion, almost equals to what Wang *et al.* [8] found from their numerical analysis of the critical temperature for the $d_{x^2-y^2}$-wave pairing. Next, we turn to the curves produced using non-zero χ_{dd}. The bottom curves of Fig. 6(a), (b) and (c) in the first column indicate that increasing the dipolar interaction on the positive side reduces the peak value and shifts the peak towards high healing length while the top curves show that increasing the dipolar interaction on the negative side increases the peak value and pushes the peak position towards low healing lengths. Thus, in our study of the critical temperature in the next section, we will always use negative χ_{dd}.

Let us now turn our attention to the "effective" interactions for the phases in the second category. Consider, first, the s-wave pairing, which, in general, is a coherent superposition between the onsite and extended s-wave pairings. Its critical temperature, the root to Eq. (43), depends on the interplay between the I_1 and I_2 coefficients in a non-intuitive fashion. It is thus quite difficult to single out, under general circumstances, the "effective" interaction responsible for the s-wave pairing. However, in the case of half filling, the off diagonal elements, s_0^1 and s_1^0, vanish so that Eq. (43) reduces to the diagonal form

$$\det \begin{vmatrix} s_0^0\left(\bar{T}\right) - 1 & 0 \\ 0 & s_1^1\left(\bar{T}\right) - 1 \end{vmatrix} = 0, \tag{63}$$

which allows us to identify, straightforwardly, that the "effective" interactions are I_1 for the onsite s-wave pairing and I_2 for the extended s-wave pairing. As illustrated in the plots in the second column of Fig. 6, in contrast to I_2, I_3, and I_4, the coefficient I_1 is a monotonically decreasing function of ξ. This is nothing more than a simple reflection of the well established fact that fermions favor the s-wave pairing more than unconventional pairings in the limit of a short healing length. As expected, in comparison with Fig. 6(e) where $U_{ff} = 0$, attractive U_{ff} enhances the onsite s-wave pairing [Fig. 6(f)] while repulsive U_{ff} suppresses or even excludes (in

the region where I_1 is negative) the onsite s-wave pairing [Fig. 6(d)].

In addition to the s-wave pairing, the second category also contains the SDW and CDW ordering. In the SDW state, fermions with opposite spins tend to be distributed in different sites, which is only possible for repulsive fermions. The phonon-induced interaction is always attractive. This explains why the effective interaction for the SDW phase, $U_{SDW} \equiv U_{ff}$, is completely determined by the s-wave interaction between fermions of opposite spins U_{ff} [Eq. (58)] and exists only when $U_{ff} > 0$. In the CDW phase, fermions of opposite spins tend to aggregate on the same site, which is only possible for attractive fermions. The phonon-induced interaction is thus the main source of the interaction responsible for the CDW phase. In addition, as shown in the last column of Fig. 6, compared to Fig. 6(h) where $U_{ff} = 0$, attractive U_{ff} [Fig. 6(g)] shall help increase the effective interaction for the CDW phase, $U_{CDW} \equiv -2U_{ind}(\mathbf{Q}) - U_{ff}$, and hence enhance CDW, while repulsive U_{ff} [Fig. 6(i)] shall help decrease U_{CDW} and hence suppress CDW. In Fig. 6(i), CDW does not exist in the region where $U_{CDW} < 0$, and dominates SDW in the region on the left side of the intercept between U_{CDW} and U_{SDW} in which $-U_{ind}(\mathbf{Q}) = U_{ff}$.

6.3. Critical Temperatures

Figures 7(a) and (b) show T_c as a function of the healing length ξ at half filling. The most prominent feature is that when χ_{dd} is tuned negative in Fig. 7(b), the critical temperatures for unconventional pairings become significantly higher than their counterparts in Fig. 7(a) where $\chi_{dd} = 0$; even the g-wave pairing, which is absent in Fig. 7(a) for the temperatures plotted, enters Fig. 7(b). The features exhibited in Fig. 7 are precisely what we expect based on the"effective" interaction analysis summarized in Fig. 6, examples of which include that both $d_{x^2-y^2}$- and p-wave pairings peak at the same healing length ~ 0.6 since both are determined by I_2, that there is an intercept between the SDW and CDW phase (which takes place at $-U_{ind}(\mathbf{Q}) = U_{ff}$), and that the peaks shift toward the lower healing length when a negative χ_{dd} is turned on.

Figures 7(c) and (d) display T_c, again at half filling, as a function of $\sqrt{U_0}$. As U_0 increases, the system, shown in Fig. 7(c) where $\chi_{dd} = 0$, changes its phase from SDW to the $d_{x^2-y^2}$-wave pairing, and then to the s-wave pairing. There is a substantial increase in T_c for pairings different from $d_{x^2-y^2}$- and s-wave pairings when χ_{dd} is tuned negative in Fig. 7(d), but this increase in T_c will not alter the sequence of phases exhibited in Fig. 7(c). The conclusion is that at half filling, the $d_{x^2-y^2}$-wave pairing always dominates all other unconventional pairings in spite of the fact that the critical temperatures for the latter may increase more dramatically than the $d_{x^2-y^2}$-wave pairing in response to an increase in $|\chi_{dd}|$ and U_0.

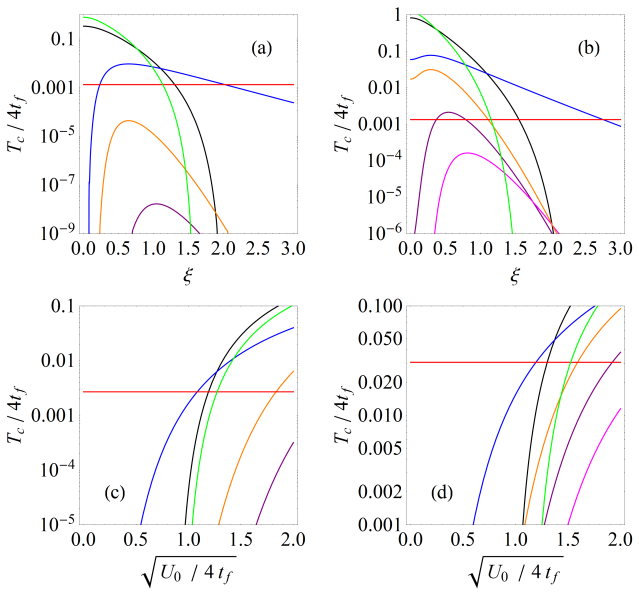

FIG. 7. (Color online) T_c as functions of the healing length ξ at half filling for (a) $\chi_{dd} = 0$ and (b) $\chi_{dd} = -0.25$ when $\sqrt{U_0/4t_f} = 1.3$ and $U_{ff}/4t_f = 0.15$. T_c as functions of $\sqrt{U_0/4t_f}$ at half filling for (c) $\chi_{dd} = 0$, $\xi = 1.0$, and $U_{ff}/4t_f = 0.18$ and (d) $\chi_{dd} = -0.25$, $\xi = 0.8$, and $U_{ff}/4t_f = 0.4$. Throughout this paper, we adopt the following color code scheme for T_c: black for s-wave, blue for $d_{x^2-y^2}$-wave, purple for d_{xy}-wave, magenta for g-wave, and orange for p-wave superfluid phases, and red for SDW and green for CDW orderings. Furthermore, for the phases of missing colors, it is implied that they either do not exist or have a T_c below the temperature scale of the relevant diagram.

Finally, we consider the effect of the filling factor n_f on T_c for various competing orders. In Fig. 8(a), we display T_c as a function of $|n_f - 1|$ for the phases in the first category when $\chi_{dd} = 0$ (solid lines) and $\chi_{dd} = -0.25$ (dashed lines). It can be seen from solid lines ($\chi_{dd} = 0$), the p-wave pairing dominates the $d_{x^2-y^2}$-wave pairing away from half filling in the region where $|n_f - 1|$ exceeds around 0.4. In the presence of χ_{dd} ($= -0.25$) (dashed lines), the crossing from the p- to $d_{x^2-y^2}$-wave pairing shifts (slightly) towards a higher $|n_f - 1|$ while the critical temperature for the p-wave pairing experiences a significant increase. Note that since both p-wave [Eq. (46)] and $d_{x^2-y^2}$-wave [Eq. (48)] pairings share the same effective interaction strength I_2, in the limit of weak interaction, the p- to $d_{x^2-y^2}$-wave crossing becomes independent of I_2 and hence is fixed essentially by the pairing symmetries. This is to be contrasted to other crossings such as from $d_{x^2-y^2}$- to d_{xy}-wave as shown by the dashed lines, which depends on the ratio of I_2 to I_3 and hence is highly susceptible to changes in system parameters.

The system is not in the p-wave state unless the p-wave pairing also has a higher T_c than the phases in the

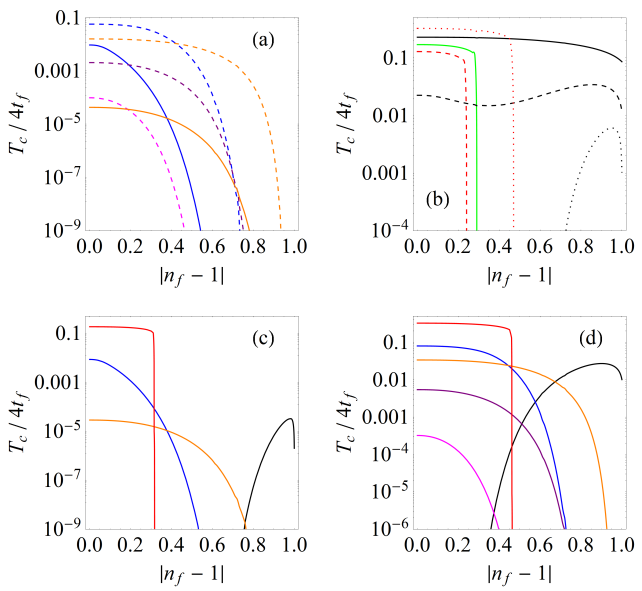

FIG. 8. (Color online) T_c as functions of $|n_f-1|$. For (a) and (b), $\xi=0.6$ and $\sqrt{U_0/4t_f}=1.3$. (a) is for the phases in the first group (with $d_{x^2-y^2}$-, d_{xy}-, p-, and g-wave pairings) with the solid and dahsed lines representing those when $\chi_{dd}=0$ and $\chi_{dd}=-0.25$, respectively. (b) is for the phases in the second group (with s-wave symmetry and SDW and CDW ordering) when $\chi_{dd}=-0.25$ and $U_{ff}=0$ (solid lines), 0.8 (dashed lines), and 1.5 (dotted lines). For (c) and (d), $\xi=0.5$ and $\sqrt{U_0/4t_f}=1.3$. (c) is for the phases when $\chi_{dd}=0$ and $U_{ff}/4t_f=1.0$ and (d) is for the phases when $\chi_{dd}=-0.27$ and $U_{ff}/4t_f=1.5$. These plots are symmetric with respect to $n_f-1\to 1-n_f$ due to the particle-hole symmetry.

second category. In Fig. 8(b), we show T_c as a function of $|n_f-1|$ for the phases in the second category under different U_{ff} (≥ 0) with the solid lines for $U_{ff}=0$, the dashed lines for $U_{ff}=0.8$, and the dotted lines for $U_{ff}=1.5$. In the absence of U_{ff} (solid lines), SDW does not exist due to the lack of repulsive interaction, CDW (solid green line) exists close to half filling due to the phonon-induced attraction, and the s-wave pairing (solid black line) has a high T_c throughout. Increasing U_{ff} suppresses CDW (not shown due to a low temperature) while enhancing and expanding SDW (dashed and dotted red lines), but most importantly it suppresses the s-wave pairing in the region of low $|n_f-1|$ (dashed and dotted black lines). This suppression is strong enough that, as shown by the dotted lines in 8(b), all phases in the second category are strongly suppressed in the same region where the p-wave pairing exceeds the $d_{x^2-y^2}$-wave pairing displayed in Fig. 8(a).

This, in turn, creates a window of opportunity for the p-wave superfluid to come out a winner. Two such examples are shown, respectively, in Fig 8(c) and (d) with and without dipolar interaction. In particular, Fig 8(d) demonstrates that the p-wave pairing with a critical temperature in the order of a hundredth of $4t_f$ is possible. The conclusion is that in contrast to the $d_{x^2-y^2}$-wave pairing, which may dominate close to half filling, the p-wave may dominate away from half filling in a window centered roughly around $|n_f-1|=0.6$, while all the other unconventional pairings, in spite of the possibility of being substantially enhanced by the use of the dipolar interaction, are unable to emerge as dominant phases.

7. Conclusion

We have considered a cold atom mixture in a square optical lattice where the mixture is made up of a two-component Fermi gas and a single-component dipolar Bose gas in the state of a homogeneous BEC. By eliminating the phonons of the dipolar BEC, we have constructed an effective lattice Fermi system which preserves the symmetry of point group D_4. Focusing on this effective model, we have explored, within the Hartree-Fock-Bogoliubov mean-field theory, the competition among density waves and superfluids with both conventional and unconventional parings. We have constructed, in the weak coupling regime, the matrix representation of the linearized gap equation in the irreducible representations of D_4. We have simplified each matrix element from a 4D integral into a separable form involving a 1D integral, which is only a function of T and μ_f, and a pairing-specific "effective" interaction, which is an analytical function of the parameters that characterize the Fermi-Fermi interactions in our system.

To help appreciate the significance of these 1D integral equations, we remind that for a continuous 3D two-component Fermi gas, there exists a similar 1D integral equation [77]

$$-\frac{2k_Fa_s}{\pi}\int_0^\infty\sqrt{x}\left[\frac{\tanh\frac{x-\bar{\mu}_f}{2\bar{T}}}{2\left(x-\bar{\mu}_f\right)}-\frac{1}{2x}\right]dx=1, \qquad (64)$$

which is the origin of the well-known formula,

$$\bar{T}\approx 8e^{\gamma-2}e^{-\pi/2k_Fa_s}/\pi, \qquad (65)$$

that one uses to estimate the critical temperature $\bar{T}$ of s-wave superfluid pairing, where k_F is the Fermi wave number, a_s the s-wave scattering length, and γ Euler-Mascheroni constant.

The 1D integral equations we highlighted in Sec. IV are analogs of Eq. (64) for fermions in a square lattice that interact via both a contact and a long-range interaction. The long-range interaction here is in the form of an attractive (lattice-version) Yukawa potential, which occurs ubiquitously across a broad spectrum of physics, e.g., nuclear physics and condensed matter physics. Thus, in analogy to Eq. (64), we expect that our 1D equations will find applications beyond the current model of interest. Further, the ability to reduce our gap equations into ones analogous to Eq. (64) may hint

that similar reductions may exist for interaction potentials with mathematical forms different from the Yakawa type. The various techniques we developed in this work may then offer a good starting point for future studies to build toolboxes for simplifying gap equations associated with such interactions.

As Eq. (64), our 1D integral equations enjoy the advantage of allowing many features of the critical temperatures to be determined in a semi-analytical manner. In particular, we have applied them to analyze the critical temperatures of various competing orders as functions of the healing length and filling factor in both the absence and presence of the dipolar interaction. We have found that tuning dipolar interaction χ_{dd} on the negative side lowers the phonon energy and can significantly enhance the unconventional pairings. We have found that close to half filling, the $d_{x^2-y^2}$-wave pairing with a critical temperature in the order of a fraction of $4t_f$ may dominate all the other phases, and at a higher filling factor, the p-wave pairing with a critical temperature in the order of a hundredth of $4t_f$ may emerge as a winner. Our theory also includes the pairings with d_{xy}- and g- wave symmetries. In spite of dramatic enhancements of their critical temperatures, we have found that tuning a dipolar interaction will not be able to make the pairings with d_{xy}- and g- wave symmetries to dominate the other phases.

It is to be stressed that the phase diagram based on the critical temperature analysis does not correspond necessarily to what is realizable at zero temperature. The actual ground state may exist as a superfluid with a pure symmetry or a coherent superposition of those with pure symmetries. [The latter dominates the phase diagram when the dipolar interaction is tuned away from the diagonal line (but stays within the square) in Fig. 2 where the system breaks D4 symmetry.] To construct the phase diagram at zero temperature requires the computational machinery of energy minimization, which can be a time-consuming task for a dipolar Bose-Fermi mixture where the parameter space is unusually large. The 1D integrals developed in this paper allow us to gain not only quick insights into various critical temperatures but also, very importantly, a sense for the role each parameter plays in this large parameter space. Thus, these integrals, just as with their 3D continuous analog in Eq. (64), serve as a valuable theoretical tool that one can use to perform a preliminary analysis before embarking on more complex tasks such as energy minimization.

Acknowledgments

B. K. is grateful to ITAMP and the Harvard-Smithsonian Center for Astrophysics for their hospitality while completing this work. H. Y. L. was supported in part by the US Army Research Office under Grant No. W911NF-10-1-0096 and in part by the US National Science Foundation under Grant No. PHY11-25915.

A. Appendix

In this appendix, we outline the main steps that we use to reduce d_0, the matrix element for the d-wave pairing, from a 4D integral in Eq. (34a) to a 1D integral in Eq. (48), and use it as an example to showcase the techniques that we employed to simplify the matrix elements for all other pairings from 4D integrals in Eqs. (32), (34) and (37) to 1D integrals in Eqs. (44), (46), (49), and (50). To begin with, we organize Eq. (34a), a 4D integral over the first Brilliouin zone in momentum space, into a 2D integral involving $S_{\mathbf{q}}(T)$

$$d_0 = \frac{1}{4(2\pi)^4}\int\int L_{\mathbf{q}} S_{\mathbf{q}}(T)\,\eta_{\mathbf{q}} d^2\mathbf{q}, \tag{A1}$$

in terms of another 2D integral involving the Fermi-Fermi interaction $U_s(\mathbf{k},\mathbf{q})$

$$L_{\mathbf{q}} = -\int\int U_s(\mathbf{k},\mathbf{q})\,\eta_{\mathbf{k}} d^2\mathbf{k}. \tag{A2}$$

As a first step to solving Eq. (A2), we substitute $U_s(\mathbf{k},\mathbf{q})$ in Eq. (29), where $U_{ind}(\mathbf{k})$ is given by Eq. (24), into Eq. (A2), and change Eq. (A2) into

$$L_{\mathbf{q}} = U_0\int\int \frac{\eta_{\mathbf{k}} d^2\mathbf{k}}{1+2\chi_{dd}+\xi^2(4-b\gamma_{\mathbf{k}-\mathbf{q}})} \tag{A3}$$

where we have used the fact that the integral involving U_{ff} is zero and the one involving $U_{ind}(\mathbf{k}+\mathbf{q})$ is the same as the one involving $U_{ind}(\mathbf{k}-\mathbf{q})$. For notational simplicity, we put Eq. (A3) in a more compact form

$$L_{\mathbf{q}} = \tilde{U}_0\int\int \frac{\eta_{\mathbf{k}} d^2\mathbf{k}}{1+\tilde{\xi}^2(4-b\gamma_{\mathbf{k}-\mathbf{q}})}$$

in terms of $\tilde{U}_0$ and $\tilde{\xi}$ defined as

$$\tilde{U}_0 = \frac{U_0}{1+2\chi_{dd}}, \quad \tilde{\xi} = \frac{\xi}{\sqrt{1+2\chi_{dd}}}. \tag{A4}$$

Next, we make the change of variables $\mathbf{k}\to\mathbf{k}-\mathbf{q}$, and by taking advantage of the integrand being a periodic function of momentum, we transform Eq. (A3) into

$$L_{\mathbf{q}} = \tilde{U}_0\int\int \frac{\eta_{\mathbf{k}+\mathbf{q}} d^2\mathbf{k}}{1+\tilde{\xi}^2(4-b\gamma_{\mathbf{k}})}, \tag{A5}$$

where $\eta_{\mathbf{k}+\mathbf{q}} = 2[\cos(k_x+q_x)-\cos(k_y+q_y)]$ or

$$\begin{aligned}\eta_{\mathbf{k}+\mathbf{q}} = {} & 2(\cos k_x\cos q_x - \cos k_y\cos q_y)\\ & -2(\sin k_x\sin q_x - \sin k_y\sin q_y).\end{aligned} \tag{A6}$$

By virtue of symmetry considerations, the integrals involving the sine functions in the second line of Eq. (A6) vanish while those involving the cosine functions in the first line of Eq. (A6) can be put into a separable form

$$L_{\mathbf{q}} = \tilde{U}_0\frac{\eta_{\mathbf{q}}}{4}\int\int \frac{\gamma_{\mathbf{k}} d^2\mathbf{k}}{1+\tilde{\xi}^2(4-b\gamma_{\mathbf{k}})}. \tag{A7}$$

To proceed, we rewrite Eq. (A7) as

$$L_{\mathbf{q}} = \tilde{U}_0 \frac{\eta_{\mathbf{q}}}{4b\tilde{\xi}^2} \left[\left(1 + 4\tilde{\xi}^2\right) L - 4\pi^2 \right], \tag{A8}$$

where L is the integral

$$L = \int\int \frac{d^2\mathbf{k}}{1 + \tilde{\xi}^2 \left(4 - b\gamma_{\mathbf{k}}\right)}, \tag{A9}$$

which we now focus on. Integrating first with respect to k_x from $-\pi$ to $+\pi$, we change Eq. (A9) into

$$L = \frac{\pi}{|b|\,\tilde{\xi}^2} \int_{-\pi}^{+\pi} \frac{dk_y}{\sqrt{\left(\cos k_y - r_+\right)\left(\cos k_y - r_-\right)}}, \tag{A10}$$

where

$$r_+ = \begin{cases} \frac{1+4\tilde{\xi}^2+2|b|\tilde{\xi}^2}{2b\tilde{\xi}^2}, & \text{if } b > 0 \\ \frac{1+4\tilde{\xi}^2-2|b|\tilde{\xi}^2}{2b\tilde{\xi}^2}, & \text{if } b < 0 \end{cases}, \tag{A11}$$

and

$$r_- = \begin{cases} \frac{1+4\tilde{\xi}^2-2|b|\tilde{\xi}^2}{2b\tilde{\xi}^2}, & \text{if } b > 0 \\ \frac{1+4\tilde{\xi}^2+2|b|\tilde{\xi}^2}{2b\tilde{\xi}^2}, & \text{if } b < 0 \end{cases}. \tag{A12}$$

We next integrate Eq. (A10) and express the result in terms of the elliptical integral as

$$L = \frac{\pi}{|b|\,\tilde{\xi}^2} \frac{4K\left[\frac{2(r_+ - r_-)}{(r_+ - 1)(r_- + 1)}\right]}{\sqrt{\left(r_+ - 1\right)\left(r_- + 1\right)}}, \tag{A13}$$

which, when r_+ and r_- are replaced with Eq. (A11) and Eq. (A12) becomes

$$L = 2\pi \frac{4}{1 + 4\tilde{\xi}^2} K\left[\frac{16b^2\tilde{\xi}^4}{\left(1 + 4\tilde{\xi}^2\right)^2}\right]. \tag{A14}$$

Finally, inserting this result into Eq. (A8), we find

$$L_{\mathbf{q}} = 2\pi^4 4t_f I_2 \eta_{\mathbf{q}},$$

expressed in terms of I_2 defined in Eq. (41b), where the use of Eq. (A4) has been made to revert back to the original notations.

Having solved $L_{\mathbf{q}}$, we now turn to d_0 in Eq. (A1), which, when $S_{\mathbf{q}}(T)$ is replaced with its scaled form in Eq. (40) becomes

$$d_0 = \frac{I_2}{2^5} \int\int S\left(\bar{\epsilon}_{\mathbf{q}}, \bar{T}\right) \eta_{\mathbf{q}}^2 d^2\mathbf{q}, \tag{A15}$$

where $\bar{\epsilon}_{\mathbf{q}} = \epsilon_{\mathbf{q},f}/4t_f = -\left(\cos q_x + \cos q_y\right)/2$. To solve this integral, we change variables from (q_x, q_y) to (c, t) via the transformation

$$c\sin t = \sin\frac{q_x}{2}, \quad c\cos t = \sin\frac{q_y}{2}, \tag{A16}$$

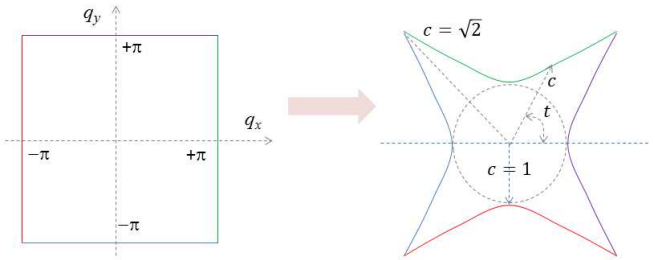

FIG. 9. (Color online) A map from the first Brillouin zone in the (q_x, q_y) plane to the polar plane where c is the radial coordinate and t is the angular coordinate. $q_x = -\pi$ is mapped to $c\sin t = -1$ (red), $q_y = \pi$ to $c\cos t = 1$ (violet), $q_x = +\pi$ to $c\sin t = 1$ (green), and $q_y = -\pi$ to $c\cos t = -1$ (blue).

which maps the first Brillouin zone, a square in momentum space, into a non-square region in the polar (c, t) plane, as shown in Fig. 9 where c is the radial coordinate and t is the angular coordinate. In terms of c and t, we have

$$d_0 = 2I_2 \int S\left(c^2 - 1, \bar{T}\right) I_t(c)\, c dc, \tag{A17}$$

where

$$I_t(c) = \int \frac{\left(c^2\cos^2 t - c^2\sin^2 t\right)^2}{\sqrt{\left(1 - c^2\sin^2 t\right)\left(1 - c^2\cos^2 t\right)}} dt. \tag{A18}$$

At this point, we turn to the Brillouin zone in the (c, t) plane in Fig. 9. Due to the symmetry inherent to $I_t(c)$, $I_t(c)$ is eight times the integral over the region from $t = \pi/4$ to $\pi/2$ in the first quadrant of the polar plane, which is divided into two areas, $\pi/4 < t < \pi/2$ if $0 < c < 1$ and $\pi/4 < t < \sin^{-1}\frac{1}{c}$ if $1 < c < \sqrt{2}$. Thus,

$$I_t(c) = \begin{cases} 8\int_{\pi/4}^{\pi/2} (\cdots)\, dt, & 0 < c < 1, \\ 8\int_{\pi/4}^{\sin^{-1}\frac{1}{c}} (\cdots)\, dt, & 1 < c < \sqrt{2}, \end{cases} \tag{A19}$$

where $(\cdots)$ is the integrand in Eq. (A18). Making a change of variables from t to $t'/2 + \pi/4$, we find, with some algebraic manipulations, that

$$I_t(c) = 8\left(2 - c^2\right) \times \begin{cases} K\left(r^2\right) - E\left(r^2\right), & 0 < c < 1, \\ F\left(\sin^{-1}\frac{1}{r}, r^2\right) - E\left(\sin^{-1}\frac{1}{r}, r^2\right), & 1 < c < \sqrt{2}, \end{cases} \tag{A20}$$

where

$$r = c^2/\left(2 - c^2\right) \tag{A21}$$

and $F(\phi, k)$ and $E(\phi, k)$ are the incomplete elliptic integrals of the first and second kind, respectively. Note that when $1 < c < \sqrt{2}$, r^2 according to Eq. (A21) is

greater than 1 so that $F\left(\sin^{-1}\frac{1}{r}, r^2\right)$ and $E\left(\sin^{-1}\frac{1}{r}, r^2\right)$ in Eq. (A20) are ill defined. This can be circumvented by making use of the identities

$$F\left[\sin^{-1}\frac{1}{r}, r^2\right] = \frac{K\left(r^{-2}\right)}{r}, \tag{A22a}$$

$$E\left(\sin^{-1}\frac{1}{r}, r^2\right) = rE\left(r^{-2}\right) + \left(\frac{1}{r} - r\right)K\left(r^{-2}\right), \tag{A22b}$$

which can be shown to hold when $r > 1$. With this, we simplify Eq. (A20) into

$$I_t(c) = 8\left(2-c^2\right) \times \begin{cases} K\left(r^2\right) - E\left(r^2\right), & 0 < c < 1, \\ r\left[K\left(r^{-2}\right) - E\left(r^{-2}\right)\right], & 1 < c < \sqrt{2}. \end{cases} \tag{A23}$$

Finally, we integrate Eq. (A17) involving the piecewise function $I_t(c)$ with respect to the radial coordinate c,

$$d_0 = 2I_2 \int_0^1 S\left(c^2 - 1, \bar{T}\right) I_t(c)\, cdc + 2I_2 \int_1^{\sqrt{2}} S\left(c^2 - 1, \bar{T}\right) I_t(c)\, cdc, \tag{A24}$$

and change it into Eq. (48) in the main text after substituting $c = \sqrt{1+x}$ and further algebraic manipulations.

[1] M. Greiner, O. Mandel, T. Esslinger, T. W. Hansch, and I. Bloch, Nature **415**, 39 (2002).
[2] M. P. A. Fisher, P. B. Weichman, G. Grinstein, and D. S. Fisher, Phys. Rev. B **40**, 546 (1989).
[3] D. Jaksch, C. Bruder, J. I. Cirac, C. W. Gardiner, and P. Zoller, Phys. Rev. Lett. **81**, 3108 (1998).
[4] I. Bloch, J. Dalibard, and W. Zwerger, Rev. Mod. Phys. **80**, 885 (2008).
[5] J. R. Schrieffer, "Theory of Superconductivity," New York: Benjamin (1964).
[6] M. J. Bijlsma, B. A. Heringa, and H. T. C. Stoof, Phys. Rev. A **61**, 053601 (2000).
[7] L. Viverit, Phys. Rev. A **66**, 023605 (2002).
[8] D.-W. Wang, M. D. Lukin, and E. Demler, Phys. Rev. A **72**, 051604 (2005).
[9] A. G. Truscott, K. E. Strecker, W. I. McAlexander, G. B. Partridge, and R. G. Hulet, Science **291**, 2570 (2001).
[10] F. Schreck, L. Khaykovich, K. L. Corwin, G. Ferrari, T. Bourdel, J. Cubizolles, and C. Salomon, Phys. Rev. Lett. **87**, 080403 (2001).
[11] Z. Hadzibabic, C. A. Stan, K. Dieckmann, S. Gupta, M. W. Zwierlein, A. Görlitz, and W. Ketterle, Phys. Rev. Lett. **88**, 160401 (2002).
[12] G. Ferrari, M. Inguscio, W. Jastrzebski, G. Modugno, G. Roati, and A. Simoni, Phys. Rev. Lett. **89**, 053202 (2002).
[13] G. Roati, F. Riboli, G. Modugno, and M. Inguscio, Phys. Rev. Lett. **89**, 150403 (2002).
[14] S. Inouye, J. Goldwin, M. L. Olsen, C. Ticknor, J. L. Bohn, and D. S. Jin, Phys. Rev. Lett. **93**, 183201 (2004).
[15] F. Ferlaino, C. D'Errico, G. Roati, M. Zaccanti, M. Inguscio, G. Modugno, and A. Simoni, Phys. Rev. A **73**, 040702 (2006).
[16] B. Deh, C. Marzok, C. Zimmermann, and P. W. Courteille, Phys. Rev. A **77**, 010701 (2008).
[17] J. W. Park, C.-H. Wu, I. Santiago, T. G. Tiecke, S. Will, P. Ahmadi, and M. W. Zwierlein, Phys. Rev. A **85**, 051602 (2012).
[18] I. Ferrier-Barbut, M. Delehaye, S. Laurent, A. T. Grier, M. Pierce, B. S. Rem, F. Chevy, and C. Salomon, Science **345**, 1035 (2014).
[19] J. Stuhler, A. Griesmaier, T. Koch, M. Fattori, T. Pfau, S. Giovanazzi, P. Pedri, and L. Santos, Phys. Rev. Lett. **95**, 150406 (2005).
[20] S. Ospelkaus, A. Peér, K. K. Ni, J. J. Zirbel, B. Neyenhuis, S. Kotochigova, P. S. Julienne, J. Ye, and D. S. Jin, Nature Phys. **4**, 622 (2008).
[21] K.-K. Ni, S. Ospelkaus, M. H. G. de Miranda, A. Pe'er, B. Neyenhuis, J. J. Zirbel, S. Kotochigova, P. S. Julienne, D. S. Jin, and J. Ye, Science **322**, 231 (2008).
[22] M. Taglieber, A.-C. Voigt, T. Aoki, T. W. Hänsch, and K. Dieckmann, Phys. Rev. Lett. **100**, 010401 (2008).
[23] A.-C. Voigt, M. Taglieber, L. Costa, T. Aoki, W. Wieser, T. W. Hänsch, and K. Dieckmann, Phys. Rev. Lett. **102**, 020405 (2009).
[24] S. Pal, M. Debatin, J. Gambari, M. Lam, J. Brachmann, and K. Dieckmann, http://meetings.aps.org/Meeting/DAMOP14/Session/B3.8 (2014).
[25] J. W. Park, C.-H. Wu, J. Schloss, Q. Wang, S. Will, and M. Zwierlein, http://meetings.aps.org/Meeting/DAMOP14/Session/B3.6 (2014).
[26] M. Vengalattore, S. R. Leslie, J. Guzman, and D. M. Stamper-Kurn, Phys. Rev. Lett. **100**, 170403 (2008).
[27] S. Ospelkaus, K.-K. Ni, M. H. G. de Miranda, B. Neyenhuis, D. Wang, S. Kotochigova, P. S. Julienne, D. S. Jin, and J. Ye, Faraday Discuss. **142**, 351 (2009).
[28] M. Lu, N. Q. Burdick, S. H. Youn, and B. L. Lev, Phys. Rev. Lett. **107**, 190401 (2011).
[29] K. Aikawa, A. Frisch, M. Mark, S. Baier, A. Rietzler, R. Grimm, and F. Ferlaino, Phys. Rev. Lett. **108**, 210401 (2012).
[30] C.-H. Wu, I. Santiago, J. W. Park, P. Ahmadi, and M. W. Zwierlein, Phys. Rev. A **84**, 011601 (2011).
[31] Y.-I. Shin, A. Schirotzek, C. H. Schunck, and W. Ketterle, Phys. Rev. Lett. **101**, 070404 (2008).
[32] L. Santos, G. V. Shlyapnikov, P. Zoller, and M. Lewenstein, Phys. Rev. Lett. **85**, 1791 (2000).
[33] S. Yi and L. You, Phys. Rev. A **61**, 041604 (2000).
[34] M. Lewenstein, L. Santos, M. A. Baranov, and H. Fehrmann, Phys. Rev. Lett. **92**, 050401 (2004).

[35] K. Sengupta, N. Dupuis, and P. Majumdar, Phys. Rev. A **75**, 063625 (2007).
[36] S. Sinha and K. Sengupta, Phys. Rev. B **79**, 115124 (2009).
[37] H. P. Büchler and G. Blatter, Phys. Rev. Lett. **91**, 130404 (2003).
[38] H. P. Büchler and G. Blatter, Phys. Rev. A **69**, 063603 (2004).
[39] P. P. Orth, D. L. Bergman, and K. Le Hur, Phys. Rev. A **80**, 023624 (2009).
[40] L.-K. Lim, A. Lazarides, A. Hemmerich, and C. Morais Smith, Phys. Rev. A **82**, 013616 (2010).
[41] L.-K. Lim, A. Hemmerich, and C. M. Smith, Phys. Rev. A **81**, 023404 (2010).
[42] L. Mathey, S.-W. Tsai, and A. H. C. Neto, Phys. Rev. Lett. **97**, 030601 (2006).
[43] F. D. Klironomos and S.-W. Tsai, Phys. Rev. Lett. **99**, 100401 (2007).
[44] W.-M. Huang, C.-Y. Lai, C. Shi, and S.-W. Tsai, Phys. Rev. B **88**, 054504 (2013).
[45] J. Bardeen, L. N. Cooper, and J. R. Schrieffer, Phys. Rev. **108**, 1175 (1957).
[46] P. W. Anderson and P. Morel, Phys. Rev. **123**, 1911 (1961).
[47] R. Balian and N. R. Werthamer, Phys. Rev. **131**, 1553 (1963).
[48] D. D. Osheroff, R. C. Richardson, and D. M. Lee, Phys. Rev. Lett. **28**, 885 (1972).
[49] J. G. Bednorz and K. A. Müller, Z. Phys. B **64**, 189 (1986).
[50] D. Scalapino, Physics Reports **250**, 329 (1995), ISSN 0370-1573.
[51] C. C. Tsuei and J. R. Kirtley, Rev. Mod. Phys. **72**, 969 (2000).
[52] R. Micnas, J. Ranninger, S. Robaszkiewicz, and S. Tabor, Phys. Rev. B **37**, 9410 (1988).
[53] R. Micnas, J. Ranninger, and S. Robaszkiewicz, Rev. Mod. Phys. **62**, 113 (1990).
[54] M. Bukov and L. Pollet, Phys. Rev. B **89**, 094502 (2014).
[55] L. Balents, private communication.
[56] K. I. Petsas, A. B. Coates, and G. Grynberg, Phys. Rev. A **50**, 5173 (1994).
[57] L. Guidoni, C. Triché, P. Verkerk, and G. Grynberg, Phys. Rev. Lett. **79**, 3363 (1997).
[58] A. Albus, F. Illuminati, and J. Eisert, Phys. Rev. A **68**, 023606 (2003).
[59] I. Titvinidze, M. Snoek, and W. Hofstetter, Phys. Rev. B **79**, 144506 (2009).
[60] C. Lin, E. Zhao, and W. V. Liu, Phys. Rev. B **81**, 045115 (2010).
[61] C. Menotti, C. Trefzger, and M. Lewenstein, Phys. Rev. Lett. **98**, 235301 (2007).
[62] I. Titvinidze, M. Snoek, and W. Hofstetter, Phys. Rev. Lett. **100**, 100401 (2008).
[63] I. Danshita and C. A. R. Sá de Melo, Phys. Rev. Lett. **103**, 225301 (2009).
[64] L. P. Gorkov and T. K. Melik-Barkhudarov, So. Phys. JETP **13**, (1961).
[65] H. Heiselberg, C. J. Pethick, H. Smith, and L. Viverit, Phys. Rev. Lett. **85**, 2418 (2000).
[66] W. Kohn and J. M. Luttinger, Phys. Rev. Lett. **15**, 524 (1965).
[67] D. V. Efremov and L. Viverit, Phys. Rev. B **65**, 134519 (2002).
[68] V. M. Galitski and S. Das Sarma, Phys. Rev. B **67**, 144520 (2003).
[69] P. G. de Gennes, "Superconductivity of Metals and Alloys," Redwood City, California: Addison-Wesley (1989).
[70] L. Landau and E. Lifshitz, "Statistical Physics," New York: Pergamon (1979).
[71] A. M. Black-Schaffer and C. Honerkamp, J. Phys.: Condens. Matter **26**, 423201 (2014).
[72] R. Gilmore, private communication (2015).
[73] M. Abramowitz and I. A. Stegun, "Handbook of Mathematical Functions with Formulas, Graphs, and Mathematical Tables," National Bureau of Standards (1964).
[74] G. Grüner, "Density Waves in Solids," Cambridge, Massachusetts: Perseus Publishing (1994).
[75] I. E. Dzyaloshinskii and V. M. Yakovenko, Sov. Phys. JETP **67**, 844 (1988).
[76] A. T. Zheleznyak, V. M. Yakovenko, and I. E. Dzyaloshinskii, Phys. Rev. B **55**, 3200 (1997).
[77] H. T. C. Stoof, K. B. Gubbels, D. B. M. Dickerscheid, "Ultracold Quantum Fields," Dordrecht, The Netherlands: Springer (2009).